Nanoscale

Accepted Manuscript

This article can be cited before page numbers have been issued, to do this please use: P. Banerjee, Y. Lin, C. E. Rowland, B. Abecassis, X. Lin, E. Shevchenko, S. Dutta, J. Wen, B. Lee, B. T. Diroll, R. D. Schaller, X. Zuo, P. C. dos Santos Claro, R. VALLEIX and B. Wagnon, *Nanoscale*, 2026, DOI: 10.1039/D6NR00826G.

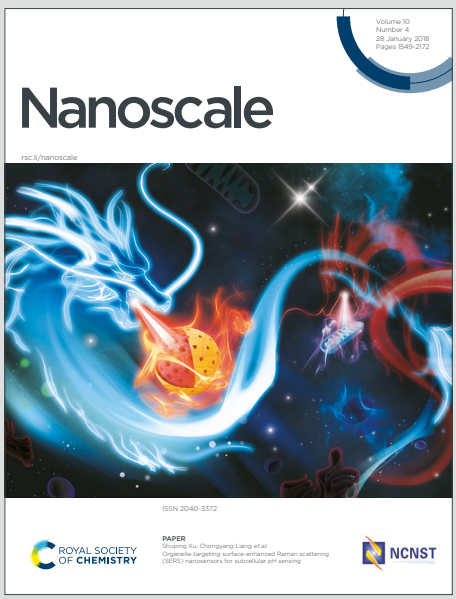

ROYAL SOCIETY OF CHEMISTRY

rsc.li/nanoscale

View Article Online
DOI: 10.1039/D6NR00826G

Strong Effect of Nonpolar Solvent Molecular Structure on CdSe Nanoplatelet Stacking

Progna Banerjee[1,2], Sarit Dutta[3], Yulin Lin[1], Jianguo Wen[1], Byeongdu Lee[4], Benjamin T. Diroll[1], Clare E. Rowland,[1] Richard Schaller[1,5], Xiaobing Zuo[4], Paula C. dos Santos Claro[1], Rodolphe Valleix[3], Benoît Wagnon[3], Benjamin Abecassis[3], Xiao-Min Lin*[1], & Elena V. Shevchenko*[1,5,6]*

[1]Center for Nanoscale Materials, Argonne National Laboratory, Lemont, Illinois 60439, USA

[2]Department of Chemistry and Biochemistry, Loyola University Chicago, Chicago, Illinois, 60660, USA

[3]Université de Lyon, ENS de Lyon, CNRS, Laboratoire de Chimie, F-69342, Lyon, France

[4]X-ray Science Division, Advanced Photon Source, Argonne National Laboratory, Lemont, Illinois 60439, USA

[5]Department of Chemistry, Northwestern University, Evanston, Illinois 60208, USA
[6]Department of Chemistry and [7]James Franck Institute, University of Chicago, Chicago, Illinois 60637, USA

** Corresponding authors: Benjamin Abecassis (benjamin.abecassis@ens-lyon.fr); Xiao-Min Lin (xmlin@anl.gov); Elena V. Shevchenko (eshevchenko@anl.gov)*

KEYWORDS. CdSe, nanoplatelets, solvent, self-assembly, ligand shell, anti-solvent, toluene, methylcyclohexane, in-situ TEM, small angle X-ray scattering, lasing, amplified spontaneous emission

ABSTRACT

We report a drastic difference in stacking behavior of oleic acid-stabilized 4-monolayer (4ML) CdSe nanoplatelets (NPLs) in toluene and methylcyclohexane (MCH), two nonpolar solvents that differ in conformational flexibility of the molecules. Using liquid cell transmission electron microscopy (TEM) and small angle scattering (SAXS) techniques, we show that NPLs form microns long ribbons consisting of 4 mL CdSe NPLs in toluene, the solvent widely used to form stable colloidal solutions of a broad range of quasi-spherical nanoparticles. In contrast, 4 ML CdSe NPLs are well-dispersed in MCH. The difference in stacking behavior of NPLs in toluene and MCH suggests that the conformational flexibility of the solvent molecule, such as the ability to adopt multiple chair conformations, modulates nanoplatelet interactions. Molecular dynamics (MD) simulations reveal how solvent molecules can alter both the ligand shell and the CdSe NPL

View Article Online
DOI: 10.1039/D6NR00826G

itself. We show that toluene better solvates the oleate ligands while MCH induces a bimodal oleate span distribution, that can lead to increased solubility of CdSe NPLs. In addition, the solvent can also influence the inorganic core, which, in turn, can modify the nanoparticle properties. We demonstrate that destabilization of toluene solution containing the ribbons of 4 ML CdSe NPLs without CdS shell results in the formation of NPL assemblies with amplified spontaneous emission (ASE) with a low threshold of 14 μJ/cm² that is comparable with that of CdSe/CdS core/shell NPLs. Our results emphasize that the solvent itself plays a major role in mediating interactions between NPLs and hence their processability for fabrication of functional structures.

INTRODUCTION

CdSe nanoplatelets (NPLs) reveal well-defined, thickness-tunable opto-electronic absorption features with ultranarrow emission bandwidth, high absorption cross-sections and high oscillator strengths.[1-4] They can therefore be used to design light-emitting diodes (LED), compact lasers, and other opto-electronic devices. [1-4] NPLs offer the advantage of solution processability,[5-7] enabling the integration of individual components into functional structures and devices.[8] The particle-particle interactions dictate the distance and interactions[9-11] between neighboring NPLs and hence affect the optical properties. As a result, the behavior of NPLs in the solution and its correlation with the structures formed *via* drying or by solution destabilization are important for designing functional structures. [3, 12-15]

Overall, significant progress has been made in understanding nanoparticle (NP) interactions by focusing on their inorganic cores, both in solution and within assembled structures.[16, 17]However, the nanoparticle surface remains difficult to probe at the molecular level, limiting quantitative insight into monolayer structure.[18] Nevertheless, a growing body of experimental evidence demonstrates that the nature of the ligands, their distribution, and their solvation,[5, 19-26] play a critical role, and that interparticle forces arising from ligand interactions can even exceed van der Waals interactions between the inorganic cores.[27, 28]

Solvent effects on the NPs' interactions were studied theoretically[23, 25, 29-33] and experimentally[23, 25, 31, 32, 34-39] mainly for three-dimensional (3D) faceted and quasi-spherical NPs. It was shown that the colloidal stability of 3.4 nm Au NPs decreased as cyclohexane > heptane > nonane > decane > toluene and suggested that details of the molecular interactions between solvent and ligand shell explain the difference.[39] It was shown that, simple cubic and body-centered-

View Article Online
DOI: 10.1039/D6NR00826G

tetragonal lattices were formed by cubic Pt NPs by evaporation of their toluene and hexane solution, respectively.[34] Also, different crystalline structure of PbS NP superlattices were fabricated from toluene and hexane solutions, respectively.[37] The difference in the formed structures was attributed to the different solubility of PbS NPs in toluene and hexane,[37] that can be connected to the fact that solvent itself affects the thickness of the ligand shell as it was recently demonstrated in detailed small angle and neutron scattering studies on PbS NPs.[28] It was also reported that ligand shell solvation changes in the presence of the a non-solvent [5, 29] which, in turn, affects the self-assembly of NPs.[40] Additionally, the preferential solvation of the ligand shell by one of the components in the solvent mixtures was demonstrated.[31] However, generally in the case of faceted or quasi-spherical NPs it is assumed that NPs stabilized with organic molecules have good solubility in nonpolar solvents unless some manipulations with colloidal solutions (typically via addition of a different surface ligands or an non-solvent) are performed; and solvents such as, for example, toluene and hexane are used regularly and considered to be replaceable with each other. The same is expected for NPs with different morphology, such as NPLs.

To date, NPLs' superstructures were reported to be formed by either destabilizing their colloidal solutions by polar solvent or solvent evaporation.[15, 41-43] For example, a multi-strand bundles of CdSe NPLs were observed upon addition of ethanol to CdSe NPLs in hexane.[12] These micrometer long, highly aligned needle like superstructures exhibit polarize emission. Also, addition of ethanol to hexane solutions of CdSe NPLs resulted in the formation of stacks of NPLs with the strong and long-range ultra efficient Förster resonance energy transfer.[44] Single-strand ribbons of stacked CdSe NPLs were formed by solvent evaporation of their colloidal solutions upon addition of oleic acid.[45, 46] It was also shown that the addition of alkyl phosphonic acids[15] or fatty acids[47] induced the assembly of CdSe NPLs into stacks in chloroform and hexane, respectively. In the case of NPLs, it is reasonable to expect stronger effect of the ligands on NPLs' themselves since the ratio of ligand shell/inorganic core is substantially larger as compared to 3D NPs[48] and hence the role of ligand shell is more dramatic.[49] It is widely acknowledged that some solvents (e.g. hexane and MCH)[7, 47, 50-52] favor the "flat" orientation of CdSe NPLs upon fast solvent evaporation while pronounced stacking of CdSe NPLs can be noticed in samples deposited from chloroform.[15] Moreover, the ligands were shown to induce surface strain, resulting in ligand-induced mechanical stress and distortion of thin NPL itself, leading to the formation of chiral ribbons upon solvent evaporation[45] or curling of NPLs into helices.[53, 54] Nevertheless, regardless

View Article Online
DOI: 10.1039/D6NR00826G

whether the studies on CdSe NPLs were focusing on their assembly via ligands' manupulation[15, 45-47] solvent composition manipulations,[12, 44] assembly kinetic effects[7] or cation exchange in CdSe NPLs,[51, 55, 56] the role of the nonpolar solvent was not considered.

Here we studied solutions of CdSe NPLs in toluene and methylcyclohexane (MCH). These two nonpolar solvents have close molecular weights but strongly differ in their molecular structures and hence conformational flexibilities. Toluene has a rigid, planar benzene ring with a methyl substituent while MCH is saturated flexible cycloalkane. Toluene is one of the most commonly used solvents to disperse different types of NPs, including NPLs[55, 57, 58] In turn, MCH is often the empirically chosen solvent to fabricate the optical devices.[50] Using liquid cell TEM and SAXS, we demonstrate the dependence of 4 ML CdSe NPLs on the solvent to form stacks or be fully dispersed, and we propose that this behavior depends on the conformational flexibility of the solvent molecules. Molecular dynamic (MD) simulations revealed important difference in surface oleate shell in toluene and MCH indicating that the structure of the ligand shell can vary with the solvent even though they are both considered "good" solvents for NPs stabilized with oleic acid. We discuss several effects such as solvent structuring or NPL twisting which can relate the differences in stacking to the structure of the monolayer. Finally, we exploit the tendency of 4 ML CdSe NPLs to form stacks to fabricate self-assembled structures with a low lasing threshold of 14 μJ/cm^2 which is comparable with the values previously reported for structures assembled from more sophisticated CdSe/CdS core/shell NPLs. We also demonstrate that 3 ML and 5 ML CdSe NPLs reveal the trends in toluene and MCH similar to 4 ML CdSe NPLs. Understating the stacking behavior of NPLs in solvents is important since it affects the chemical reactivity of NPLs, self-assembly of NPLs into hierarchical structures and performance of NPLs based functional structures fabricated via solution processing.

RESULTS AND DISCUSSIONS:

The 3, 4 and 5 ML (ML is defined with respect to the total Se layers[2,4]) thin CdSe NPLs were synthesized according to the previously reported method.[59] The experimental details are presented in Supporting Information (**Figure S1**). We primarily used 4 ML CdSe NPLs, the most widely studied system, to examine solvent effects on NPL interactions and to connect our results with previously reported data. Additionally, we conducted experiments using 3 ML and 5 ML CdS NPLs in toluene and MCH. We dispersed equivalent amounts of the purified 4 ML CdSe NPLs

View Article Online
DOI: 10.1039/D6NR00826G

with lateral dimensions of ~24 nm×8 nm (**Figure 1**) in MCH and toluene. CdSe NPLs underwent exactly the same purification steps prior to their dissolution in MCH and toluene to have the same concentration of oleate ligands in both solvents in order to minimize the effects associated with the different ligand coverage.[60] Toluene and MCH were chosen as model systems of solvent molecules with different molecular geometries for two reasons: (i) toluene is one of the most common solvents for all NPs synthetizes in nonpolar solvents and (ii) they MCH and toluene have higher boiling temperatures (~101°C and 111 °C, respectively) than cyclohexane (~81.74 °C) and hexane (~69 °C), another common solvent for colloidal NPs. The higher boiling points of MCH and toluene enable reproducible liquid cell TEM studies.

We first analyzed the 4 ML CdSe samples deposited by the fast evaporation of their toluene and MCH solutions using conventional TEM. **Figure 1a shows** that, in the sample obtained by drying MCH solution, NPLs are randomly oriented but aligned parallel to the substrate. In contrast, periodic stacks of NPLs oriented perpendicular to the substrate are observed in the case of samples deposited from toluene (**Figure 1b**). Previous studies suggest that in the case of NPs with different morphologies, the assembly of NPs is induced by solvent evaporation of the colloidal solutions of NPs randomly distributed in solvent.[45, 61 12, 37, 47, 62-64] The differing TEM drying behavior of 4 ML CdSe NPLs from toluene *vs* MCH points out that solvent-dependent interparticle forces in solution. The optical absorbance data show no differences in the position of the heavy-hole (*hh*) excitons in toluene and MCH (**Figure 1c)**; however, the UV/Vis spectrum in toluene has a higher background than in MCH, which can be indicative of light scattering (**Figure 1c**). Interestingly, the maximum of the PL spectrum of CdSe NPLs in toluene is red shifted by 3 nm, which can indicate energy transfer or re-absorption effects from path length elongation from scattering (**Figure 1d**). Moreover, small-angle X-ray scattering (SAXS) data show a substantial degree of ordering of CdSe NPLs in toluene dispersions, evidenced by the presence of two sharp peaks at q of 0.117 $Å^{-1}$ and 0.233 $Å^{-1}$ in the corresponding SAXS diagrams (**Figure 1e**). In contrast, the SAXS pattern in MCH shows only a hump around 0.115 $Å^{-1}$ indicating only traces of ordering (**Figure 1e**). The same features are visible in the SAXS patterns of 5 ML CdSe NPL in these two solvents. Stacking peaks at 0.11 and 0.22 $Å^{-1}$ in toluene indicate a lamellar ordering,[47] while the featureless SAXS pattern of 5 ML CdSe dissolved in MCH proves that the NPLs are randomly dispersed in this solvent (**Figure S2a**). While the stacks observed in TEM for toluene in **Figure 1b** could result

View Article Online
DOI: 10.1039/D6NR00826G

from evaporation induced self-assembly on the TEM grid, optical and SAXS data (**Figures 1c-e**) point towards stacking in solution prior to evaporation.

Motivated by the observation of the presence of long-range ordering in toluene solutions of CdSe NPLs and different packing of NPLs deposited from MCH and toluene (**Figure 1**), we decided to conduct the in-situ TEM study in liquid cells. In these experiments, a droplet of NPL solution was sandwiched between two amorphous carbon sheets. The sealing of the liquid cells was adjusted to enable evaporation in areas close to the seal. The in-situ TEM experiments revealed the well dispersed CdSe NPLs in MCH and the presence of tens of microns long ribbons consisting of 4 mL CdSe NPLs in toluene (**Figures 2**). Interestingly, at the edge of the droplet (**Figures 2e, f**), evaporation of the solvent was associated with breaking ribbons into smaller fragments, as is evidenced by TEM images in the dried area of the liquid cell. **Figures S3** and **Figures S4** show similar trends in 4 ML CdSe NPLs from different batches. Other studies also reported similar images of the stacks of 4 mL CdSe NPLs deposited from toluene solutions.[5, 34] Liquid cell TEM data are in agreement with SAXS, UV/Vis and TEM data obtained for dried samples: toluene induces a strong stacking of the NPL in solution while they are well dispersed in MCH.

Toluene and MCH have similar Hansen solubility parameters (HSPs): 18.165 $MPa^{1/2}$ and 16 $MPa^{1/2}$, respectively.[65] Recent studies report that the HSP of oleic acid is between 17.21 $MPa^{1/2}$ and 18.74 $MPa^{1/2}$, [66 67] higher values than earlier reported 15.6 $MPa^{1/2}$. [68] The smaller difference between the Hansen solubility parameters of two substances, the better their better solubility.[5] In this perspective, the oleic acid shell should be slightly more solvated in toluene even though the difference is not that pronounced. However, the HSP considers solubility in bulk which includes the interactions between the headgroup and the solvent. In our case, the carboxylate group is bound to the NPL surface, and the observed difference is likely to come from the interplay between the carbon ligand backbone of the ligand chain and the solvents.

Previously, it was computationally shown that hexane and toluene are both "good" solvents of 4 nm cuboctahedra PbSe NPs stabilized with oleic acid and penetrate the ligand shell all the way to the NP surface with ~3 ligands/nm^2 grafting densitities.[25] The study revealed slightly more toluene molecules than hexane for a given radial distance from the center in the oleate shell.[25] To gain more insight into solvents effects into oleate ligand shell of CdSe NPLs, we performed MD simulations on 4 ML CdSe NPs capped with oleates with grafting density of ~3.27 ligands/nm^2 in MCH and toluene (see Methods section for details)**.** We described solvent explicitly to account for

View Article Online
DOI: 10.1039/D6NR00826G

the molecular details of the interaction between the ligand brush and the solvent even though explicitly modeling the solvent is computationally demanding because it requires accounting for many additional atoms; however, as it is shown below, it yields valuable insights.

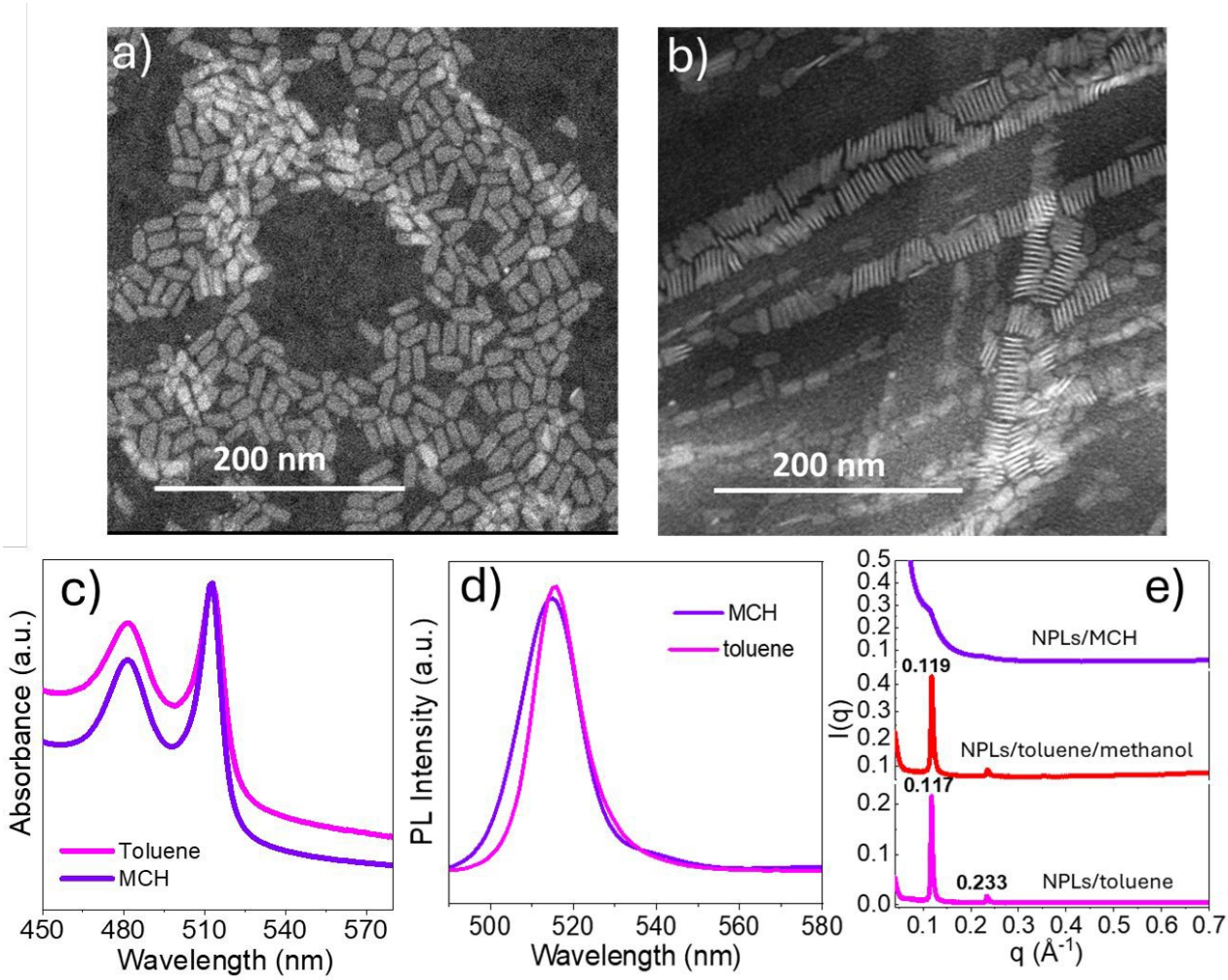

Figure 1. *Dark-field STEM images of 4 ML (monolayer) CdSe NPLs deposited from MCH (a) and toluene (b) solutions. Optical absorption (d) and PL emission (d) spectra for 4 ML CdSe NPLs dispersed in toluene and MCH. The SAXS spectra (e) measured for 4 ML CdSe NPLs dispersed in MCH, in toluene and toluene mixture with 25% methanol.*

Figure 3a depicts the relevant parameters that capture the conformation of the oleate ligand at the surface of NPLs. The span is defined as the vertical distance between the atoms in the molecule that are the farthest apart and R_{ee} is the end-to-end distance i.e. the distance between the

View Article Online
DOI: 10.1039/D6NR00826G

atom attached to the surface and the last atom of the carbon chain C_{18}. These parameters provide a quantitative description of the ligand molecules conformation at the surface. **Figure 3b** shows the density profiles of the ligand layer in the absence of a solvent, in toluene and MCH. The density profiles for toluene and MCH are similar, and very close to that in the absence of a solvent. This is expected, as the ligands are typically tightly bound to the surface Cd atoms. There are several sharp peaks close to the NPL surface, which, based on their locations, likely originate from the atoms of the binding group. However, our calculations revealed more extended ligand shells in toluene than in MCH with the maximum of the distribution of span and R_{ee} at larger distances in toluene: the R_{ee} parameter of oleates at CdSe NPL's surface is longer by ~0.53 Å in toluene than in MCH. The difference in the maximum span parameters of oleate ligand in toluene and MCH is ~0.43 Å. Therefore, the span and R_{ee} parameters are indicative of a slightly more extended ligand shell at the surface of CdSe NPLs in toluene.

It is worth noting that larger ligand shell thickness in toluene than in cyclohexane (15.6 Å and 14.8 Å, respectively) and larger volume fractions of solvent within the monolayer for toluene than for cyclohexane were recently reported for oleyl-caped PbS spherical NPs.[28] These results agrees with our atomic simulations. Indeed, the density profile of solvent inside the monolayer displays two peaks in the case of toluene: one sharp peak with a maximum very close to the NPL surface at 2 Å and a broader shoulder with a maximum at 7 Å. In contrast, the solvent density increases monotonically for MCH. We believe this is due to the different steric profiles of the two molecules: toluene can easily slip between the hydrocarbon chains of the monolayer while the chair conformation of MCH is bulkier. It is also possible that the moderate polarity of toluene makes it more compatible with interfacial region which bares carboxylate groups. A surprising feature of our simulations is the bimodal character of the span and R_{ee} probability distribution. For MCH, the span distribution displays two maxima with the same height at 14.6 and 15.2 Å (**Figure 3c**). The R_{ee} distribution shows a dominant primary mode at 17.1 Å and a secondary mode of lesser magnitude at 16.8 Å (**Figure 3d**). The same features are observed with toluene except that the two peaks in the span distribution are closer and appear like a broader monomodal distribution with a plateau between 15.6 and 16 Å.

View Article Online
DOI: 10.1039/D6NR00826G

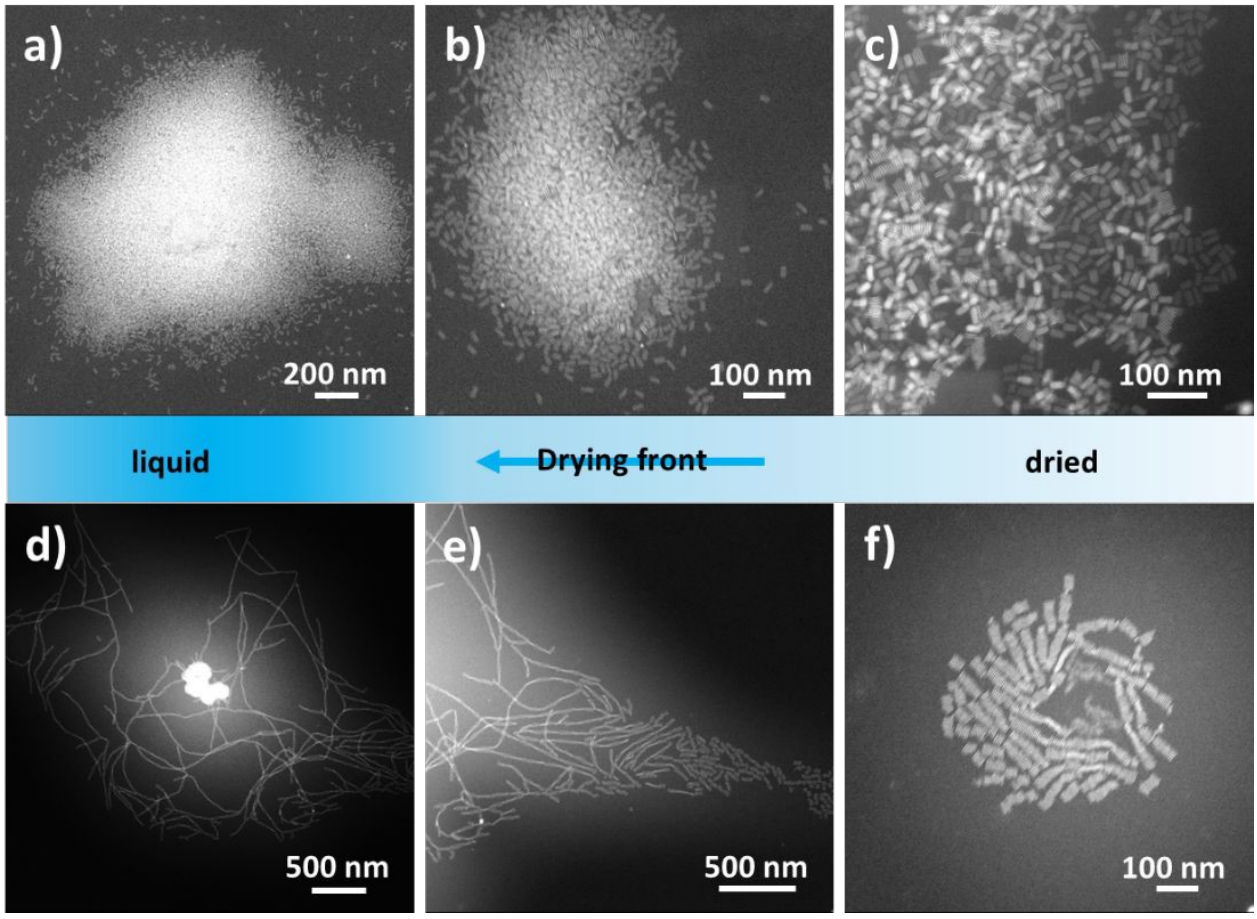

Figure 2. *Dark-field STEM images of 4 ML CdSe NPLs in MCH (a-c) and toluene (d-f) measured in liquid cell upon drying of corresponding solutions.*

The MD calculations indicate slightly more extended ligand conformations for oleate molecules on 4 ML CdSe nanoplatelets in toluene, as reflected by larger spans and end-to-end distances (R_{ee}) (**Figures 3c, d**). Previous studies have reported a correlation between ligand chain length and nanoparticle solubility in nonpolar solvents. For example, Au nanoparticles stabilized with longer-chain ligands (dioctadecylamine) exhibit higher dispersion stability than those capped with shorter ligands such as didodecylamine and dioctylamine.[69] Similarly, CdSe NPs capped with undec-10-enoic acid show lower solubility in toluene compared to those stabilized with the longer oleic acid.[70]

However, this trend is not universal. MD simulations have shown that 5 nm Au nanoparticles stabilized with C_{18} alkanethiol can exhibit lower stability against aggregation at 300 K compared

View Article Online
DOI: 10.1039/D6NR00826G

to those capped with shorter C_{12} alkanethiol.[32] Notably, in that study the ligand grafting density (~5.5 ligands/nm²) was sufficiently high to limit solvent penetration into the ligand shell.[25, 32] It has been previously demonstrated that at such high grafting densities (>4.5 ligands/nm²), solvent accessibility is significantly reduced, which alters interparticle interactions.[25] Therefore, discrepancies in reported trends can be attributed to variations in grafting density, nanoparticle size, ligand chemistry, and solvent accessibility.

Consequently, the trends in ligand extension observed in **Figures 3c** and **3d** cannot be directly mapped onto prior studies, and the experimentally observed stacking of 4 ML CdSe nanoplatelets in toluene cannot be explained solely by ligand length. Instead, we observe a pronounced difference in the distribution of oleate spans between methylcyclohexane (MCH) and toluene (**Figure 3d**). Importantly, previous studies have shown that areal partitioning of ligands with different chain lengths (e.g., myristate (C_{14}) and hexanoate (C_6)) on nanoparticle surfaces, associated with increased rotational freedom, can enhance nanoparticle solubility by up to six orders of magnitude.[70]

Although solvent-induced fluctuations in ligand spans are unlikely to produce a repulsive barrier comparable to that arising from chemically defined heterogeneity in mixed-ligand systems,[70] the dramatic solubility enhancement observed in such systems suggests that even subtle variations in ligand conformations may play a role. In this context, a modest difference in ligand spans (~0.7 Å) may still influence the solubility of CdSe nanoplatelets. We, therefore, propose that solvent-induced fluctuations leading to a bimodal distribution of ligand spans, even with a small amplitude (~0.7 Å) in span observed in MCH may contribute to the experimentally observed higher solubility of 4 ML CdSe NPLs in MCH compared to toluene.

View Article Online
DOI: 10.1039/D6NR00826G

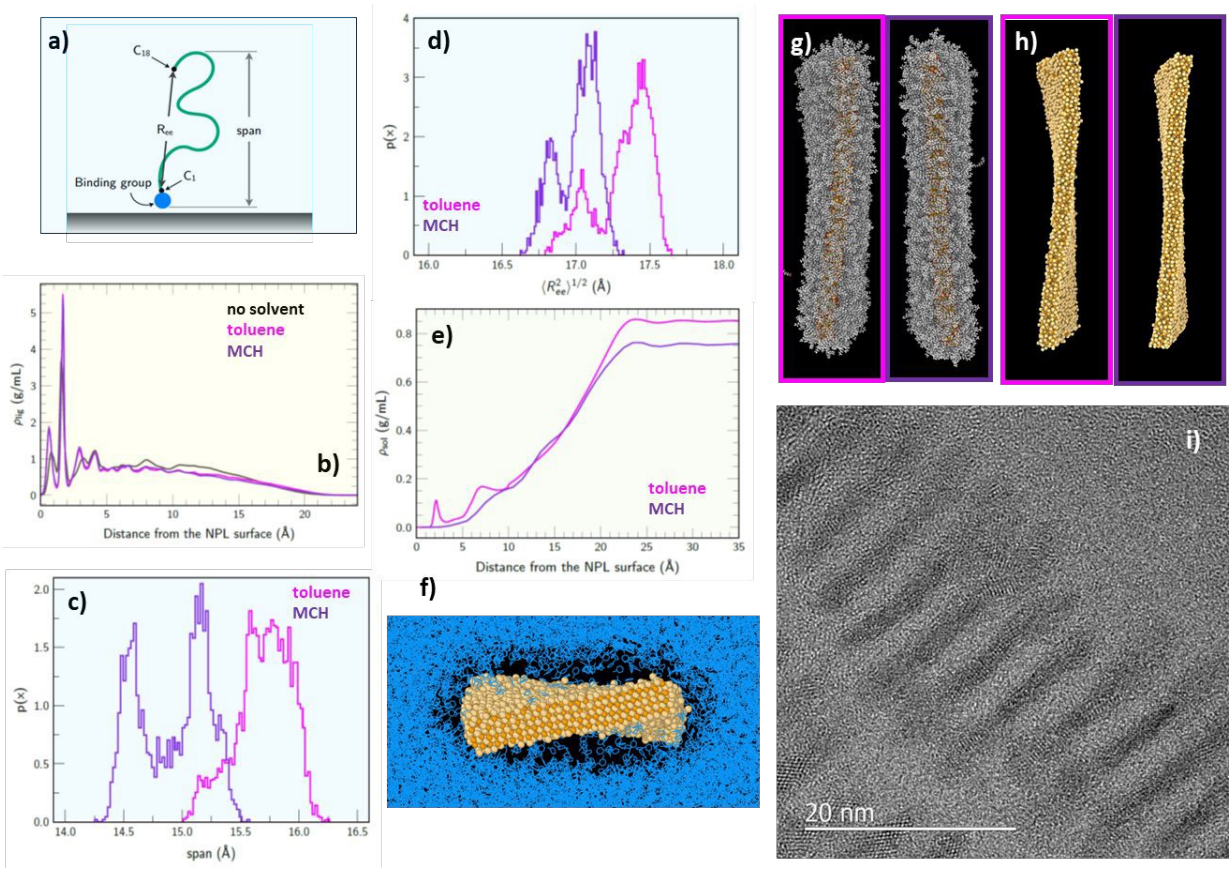

Figure 3. *(a) Depiction of the ligand at surface of NPLs demonstrating the characteristic parameters of the ligand such as end-to-end parameter (R_{ee}) and span; (b) density profiles of oleate ligands normal to the 4 ML thick CdSe NPL surface in the absence of any solvent and in the presence of toluene and MCH. (c) Span of oleate ligands as a function of distance from the 4 ML thick CdSe NPL's surface. (d) Dependance of the parameter characterizing the distance between the end group of the ligand and the group attached to the NPL's surface (R_{ee}). (e) Density profiles of solvents in oleate ligands. (f) MD simulation snapshot of a 4 ML 24 nm × 8 nm rectangular NPL in toluene with stripped ligands demonstrating the arrangement of toluene molecules with respect to the inorganic 4 ML CdSe NPL (viewed along the short in-plane dimension) ; MD simulation snapshot of a 4 ML 24 nm × 8 nm rectangular NPL in toluene (left) and MCH (right) coated with oleate ligands and with only the CdSe core shown (g and h, respectively, viewed along the long-in-plane dimension). (i) HRTEM image of 4 ML CdSe NPLs deposited from toluene.*

It is worth noting that larger ligand shell thickness in toluene than in cyclohexane (15.6 Å and 14.8 Å, respectively) and larger volume fractions of solvent within the monolayer for toluene than for cyclohexane were recently reported for oleyl-caped PbS spherical NPs.[28] Also, larger number of toluene than hexane molecules was These results agrees with our atomic simulations. Indeed,

View Article Online
DOI: 10.1039/D6NR00826G

the density profile of solvent inside the monolayer displays two peaks in the case of toluene: one sharp peak with a maximum very close to the NPL surface at 2 Å and a broader shoulder with a maximum at 7 Å (**Figure 3e**). In contrast, the solvent density increases monotonically for MCH (**Figure 3e**). We believe this is due to the different steric profiles of the two molecules: toluene can easier slip between the hydrocarbon chains of the monolayer while the chair conformation of MCH is bulkier. It is also possible that the moderate polarity of toluene makes it more compatible with interfacial region which bares carboxylate groups.

While agglomeration of larger NPs is primarily driven by van der Waals attractions between inorganic cores, ligand–ligand interactions are recognized as the dominant attractive forces at smaller sizes. [71-74] Studies on Au NPs showed a crossover near ~7.4 nm, below which interparticle interactions are ligand-shell dominated. For few-monolayer-thick CdSe NPLs, the effect is even more pronounced: the Hamaker constant of CdSe is ~ one-third that of Au,[75] making the ligand contribution especially significant.[76] Consequently, solvent-induced changes in ligand solvation can play a decisive role in governing interactions and assembly. Previously, MD simulations on cube-octahedral-shaped NPs with oleic acid shells also revealed more toluene molecules than hexane in the oleic acid corona.[25] It was proposed that the π–π interactions between the toluene rings are stronger than the ligand toluene interaction resulting in stacking of the toluene molecules in order to maximize their interactions.[25] More rigid toluene molecules, that have only limited flexibility due to their methyl groups, "lock" the surface ligands, decreasing their conformational entropy. This explanation aligns with previously reported demonstration of the correlation between the rotational freedom of the surface ligands and solubility of NPs.[77] Our results agrees with the hypothesis that more toluene molecules can be accommodated within the oleate ligand corona[25] as compared to solvent molecules with more flexible structures (e.g. MCH or hexane). It is worth noting that the TEM results reported for purified NPLs deposited from hexane,[45] whose molecules also exhibit high conformational flexibility, are similar to those we obtained from MCH (**Figure 1a**): in both cases, the NPLs are randomly distributed and oriented parallel to the substrate.[78]

MD simulations revealed another interesting feature that can be relevant to stacking NPLs: they are not flat but twisted. Significant deformations are observed for 4 ML CdSe (**Figures 3g**,**h and Figures S5-S8)** in MD simulations for both toluene and MCH but with a larger magnitude for toluene than for MCH as quantified by the average pitch of the helix which is smaller for toluene

View Article Online
DOI: 10.1039/D6NR00826G

(259 nm) than for MCH (452 nm). MD simulation snapshot visualizing how toluene molecules arrange themselves relative to the surface of 4 ML CdSe NPLs is shown in **Figure 3f**. The structure of 4 ML CdSe NPLs has been extensively studied and is generally assigned to the zinc blende phase.[79, 80] Twisting of zinc blende 4 ML CdSe NPLs with a pitch of approximately 400 nm has previously been observed in "dry" samples prepared in the presence of oleic acid ligands.[45] **Figure 3i** and **Figure S9** present HRTEM images of 4 ML CdSe NPLs deposited from toluene, which preferentially orient on their edges, revealing pronounced twisting and associated lattice distortions. These observations are in good agreement with the trends observed in MD simulations.

Such a large effect of the solvent on the shape of the crystal is surprising at first glance, but can be rationalized within the framework of incompatible curvatures developed by Monego et al.[54] It was shown that NPL could be described as elastic ribbons whose effective curvature is proportional to the curvature imposed at the ligand NPL interface.[54] In other words, the ligand monolayer imposes a curvature at the top and bottom surfaces of the NPL that depends both on the NPL/ligand interactions and on the lateral interaction between ligand tails.[54] Solvent penetration can significantly modify ligand-ligand interactions, thereby affecting the NPL curvature. A solvent that penetrates more deeply into the ligand layer, for instance, pushes the ligand tails further apart, increasing the lateral strain at the interface and ultimately driving a larger curvature of the NPL. This trend is confirmed experimentally by measuring the curvature of thinner NPL in solution for MCH and toluene.

The small lateral extension of the 4ML NPL preclude the measurement of curvature by SAXS.[81, 82] However, we measured in both solvents the SAXS pattern of 3ML NPLs with larger lateral dimensions (**Figure S2b**). The oscillations in the SAXS intensity are shifted towards lower wave vectors in MCH than in toluene. As established in earlier study,[81] a shift toward lower wavevectors in the SAXS oscillations corresponds to an increase in the radius of curvature, i.e. flatter NPLs. The 3 ML NPLs are, therefore, flatter in MCH than in toluene, which is qualitatively consistent with our MD simulation results. The solvent effect on curvature is likely more pronounced for 3ML NPLs than for 4ML NPLs owing to their smaller thickness.

NPL curvature can affect their self-assembly by inducing large permanent dipole moments. Although the zinc blende structure of CdSe is nonpolar in the bulk, atomic displacements away from equilibrium lattice positions break the local symmetry and create a charge imbalance, endowing curved NPLs with a permanent ground-state dipole.[83] This dipole moment grows with

View Article Online
DOI: 10.1039/D6NR00826G

curvature, as more pronounced bending stretches the crystal lattice further from its equilibrium configuration. Stronger dipole moments, in turn, enhance inter-NPL attraction through Keesom dipole-dipole interactions, which have been shown to be of comparable magnitude to other interactions in nanoparticle systems.[84] We estimated dipole moments from the atomic positions and partial charges extracted from the MD simulations. As expected, flat NPLs prior to crystal relaxation yield a dipole of exactly zero, since all partial charges compensate perfectly. After relaxation, the calculated dipole moments are 1063 ± 230 D in toluene and 678 ± 136 D in MCH, reflecting the larger curvature adopted by NPLs in toluene. These values correspond to dipole densities of 2–3 D/nm³, that is in a good agreement with the order of magnitude measured experimentally by transient birefringence.[83]

Therefore, both entropic effects induced by solvents in ligand shells and bending of CdSe NPLs can contribute to the difference in stacking behavior observed in MCH and toluene. While additional studies are required to quantify these contributions and their coupling, both drive 4 ML CdSe NPLs toward stacking, with toluene preferentially promoting stack formation.

The propensity of CdSe NPLs to form micrometer-long stacks in toluene motivated us to explore how this behavior can be harnessed for device fabrication. Prior work has pursued solution-processed strategies to build functional architectures, particularly low-threshold lasing structures, including tightly packed CdSe-based core–shell NPLs that reduce optical scattering and raise the effective refractive index.[85-90] Because 4 ML CdSe NPLs readily stack in toluene yet remain colloidally stable for weeks without precipitation, we investigated their use in forming three-dimensional optically active structures.

We applied a controlled oversaturation approach that was previously utilized for quasi-spherical and rod-like NPs,[5, 41-43] by destabilizing toluene dispersions of 4 ML CdSe NPLs with methanol. It is worth mentioning that in control experiment introducing 25 vol% methanol yielded sharp lamellar reflections in the SAXS pattern, confirming NPL stacking (**Figure 1e**). We also observed the shift of the primary peak from q ≈ 0.117 Å^{-1} to 0.119 Å^{-1} indicating a decrease in inter-NPL spacing in the presence of methanol (**Figure 1e**)

View Article Online
DOI: 10.1039/D6NR00826G

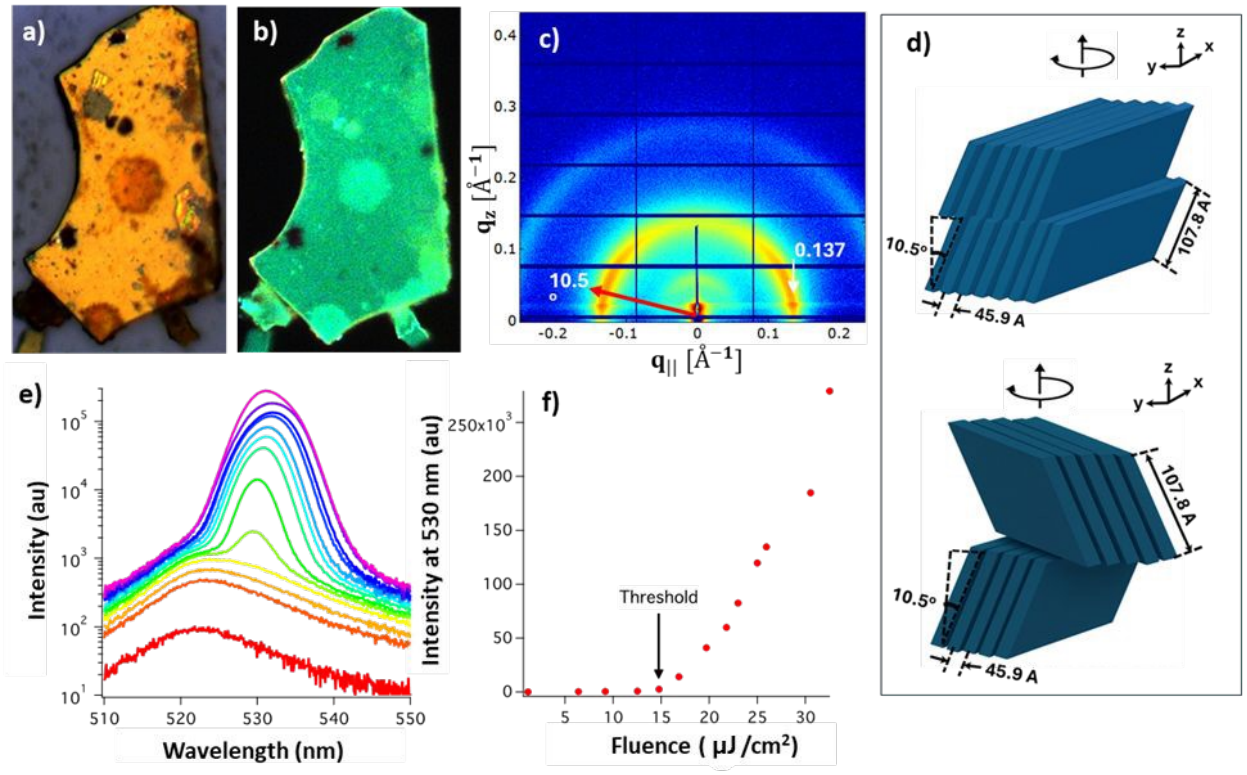

Figure 4. *Optical (a) and photoluminescence (b) images of film formed via destabilization of toluene solution of 4 ML CdSe NPLs by methanol; (c) two-dimensional SAXS pattern measured on self-assembled 4 ML CdSe NPLs shown in (a); (d) depiction of possible arrangement of 4 ML CdSe NPLs in the film; (e) emission spectra of 4ML CdSe NPLs' film at different pump fluence at room temperature; (f) normalized integrated emission intensity from the 4ML CdSe NPLs' film as a function of pump fluence at room temperature.*

To grow superlattices, a 2 mL solution of CdSe NPLs in toluene (~7 mg/mL) was placed in a crystallization tube containing a glass strip. A 2 mL layer of methanol was carefully added to avoid intermixing, and the tube was sealed. Density of the toluene (0.867 g/cm^3) is higher than the density of methanol (0.792 g/cm^3) and therefore the formation of the aggregates took place mainly below the toluene/methanol interface. After two weeks, a uniform solid film of CdSe NPLs formed along the tube walls and the glass strip below the toluene/methanol interface. Large film fragments of microns in size were easily delaminated using a metal needle (**Figures 4a and 4b**). It is worth noting that the destabilization of the MCH solution of 4 ML CdSe NPLs by either methanol or isopropanol also results in the formation of stacks (**Figure S10**). This observation agrees with previously reported assembly CdSe NPLs in hexane induced by methanol or ethanol.[12, 44] Note, MCH solution of 4 ML CdSe NPs was placed above the non-solvents since the density of MCH

View Article Online
DOI: 10.1039/D6NR00826G

(0.770 g/cm^3) is lower than the density of both methanol and isopropanol (0.786 g/cm^3) (**Figure S10**). It is also worth noting that these stacks form the gel-like structure that makes them less suitable for optical studies as compared to solid assemblies prepared by destabilization of toluene solution.

SAXS data from the films on glass strips deposited by stabilization of toluene solution of 4 ML CdSe NPLs with methanol were collected under the reflection geometry, known as grazing incidence SAXS (GISAXS). The incident angles used in this work were 0.2 ~ 0.5 degrees, which are higher than the critical angle of the substrate, to avoid x-ray refraction while taking advantage of the long footprint. For simplicity, we will refer GISAXS to SAXS since our data do not present any grazing incident effect.

The SAXS data shown in **Figure 4c** demonstrates well-resolved diffraction pattern characteristic to structures with preferred orientation of CdSe NPLs; however, the overall crystalline character is more random as compared to superlattices formed by quasi-spherical NPs[91] as it is evident by a presence of rather broad arcs in SAXS pattern. The center of the broad azimuthal arc is not in the lateral direction, or the $q_{||}$ axis, but it is tilted more than 10 degrees. In addition to those peaks due to the NPL stacking, there is another arc centered at 90 degrees in the smaller q region at q of ~ 0.0583 Å^{-1}, indicating the layering of NPL stacks along the film normal direction. No lateral peaks are found, indicating the ribbons are not oriented parallel to each other so well in each layer. **Figure 4d** depicts the possible arrangements of 4 ML CdSe NPLs within the film that can be reconstructed based on SAXS data. We do not expect correlation between NPLs CdSe NPLs are arranged on the edge tilted by ~10.5 degrees with respect to the substrate. The center-to-center distance is ~45.9 Å and therefore the interparticle spacing is ~32.9 Å given the thickness of 4 ML CdSe NPLs to be ~13 Å. From the peak width along the q direction, the coherent length in self-assembled sample is estimated to be ~6 layers. The center-to-center distance between neighboring NPLs in films is smaller than that in free-standing ribbons in toluene in the presence of methanol (~52.7 Å).

Inspired by previous studies reporting the lasing on CdSe NPLs assemblies,[1-4, 89] we investigated if we could observe amplified spontaneous emission (ASE) phenomenon in our structures. The films of 4 mL CdSe NPLs were excited with frequency-doubled pump pulses from an amplified Ti:sapphire laser system, focused on a stripe along the sample. When the pump fluence exceeded 14 μJ/cm^2, a narrow peak appeared due to ASE (**Figure 4e**). Lower ASE

View Article Online
DOI: 10.1039/D6NR00826G

threshold values were previously reported only for more sophisticated NPLs such as CdSe/CdS core/shell NPLs [2, 85, 89, 92, 93] The intensity of ASE peak increases rapidly with pump fluence (**Figure 4f**). The CdSe NPLs have well studied polarized emission related to their transient dipoles.[6, 83, 87, 94] We believe that by destabilization of toluene solution containing stacks of 4 ML CdSe NPLs by methanol, we generate the structures with lower inhomogeneity of amplified wave. Since the stacks of the NPLs is a structure with aligned dipoles it is reasonable to suggest that dipoles alignment can be responsible for the lasing in the self-assembled structures. This observation agrees with recently published data on the role of the dipole alignment of the NPs in generation of polarized emission.[95] The alignment of the dipole moments of $CsPbBr_3$ NPs in superlattice structure was reported to result in a macroscopic polarization effect producing a net polarization in the direction of the alignment, resulting in spontaneous linear polarized emission.[95] After ~6 months of storing at room temperature under nitrogen, the self-assembled films stopped demonstrating ASE, and SAXS data revealed a significant change in the ordering of NPLs (**Figure S6**). Instead of one peak at q of ~0.137 $Å^{-1}$, the samples started to reveal two broad split peaks at ~0.131 $Å^{-1}$ and ~0.155 $Å^{-1}$, respectively without any preferred orientation, and the peak from the packing of ribbons is no longer observed (**Figure S11**). These changes are indicative to the rearrangement of the CdSe NPLs in the self-assembled structures. Because the GISAXS measurements were performed on oriented films, we cannot exclude a geometrical (projection) effect. For example, when a stack of d-spacing 48 Å, corresponding to q of ~0.131 $Å^{-1}$, is tilted by 32 degree, its d-spacing would decrease to 40.5 Å, corresponding to 0.155 $Å^{-1}$. The SAXS pattern of the stored samples demonstrates stacks of smaller number of NPLs, randomly oriented without any stack-to-stack correlation (**Figure S11**). The peak broadening suggests a distribution of spacings and/or orientations, which may arise from bending, fragmentation, or slipping between neighboring CdSe NPLs. An increase in interparticle spacing may originate from the solvent loss from the ligand shell. Interestingly, as indicated by the MD simulations, in toluene the maximum end-to-end distance (R_{ee}~17.4 Å) of oleate molecules exceeds the corresponding span (~15.7 Å) (**Figures 3c, d**). This suggests that solvent evaporation may be accompanied by relaxation of the ligand chains into more extended conformations, leading to an expansion of the effective ligand shell. Consistent with this interpretation, we have previously demonstrated for PbS nanoparticles capped with oleic acid that expulsion of toluene results in a more extended ligand shell.[5] In line

View Article Online
DOI: 10.1039/D6NR00826G

with this structural perturbation, no ASE was observed following the transformation that directly points out to the correlation between structure of assembled CdSe NPLs and ASE.

It is worth noting that we also did not observe ASE in samples prepared by fast drying of the toluene solutions. Such samples are characterized by larger interparticle spacing as it is indicated by signal of q of ~0.129 $Å^{-1}$ and smaller coherent length (~4 layers). Also, the stack layering peak was not observed. The representative SAXS pattern of the sample prepared via fast drying of toluene solution is shown in **Figure S12**. Even though the SAXS pattern shows a very sharp diffraction peak characteristic to the NPL stacking (**Figure S12**), it does not show ribbon packing or layering peak at all that was present in SAXS spectrum of self-assembled structures demonstrating lasing.

CONCLUSIONS

Our results indicate that the solvation of the ligand shell itself can play a significant role, and this effect can go beyond the just effect of increased or decreased concentrations of the solvent molecules in the ligand shell. We attribute this difference to the higher flexibility of MCH molecules as compared to toluene molecules. The cyclohexane ring in MCH introduces conformational flexibility allowing to adopt different chair conformations and increasing the number of possible molecular arrangements. In contrast, planar toluene molecules with rigid aromatic structures do not exhibit the same level of conformational freedom as MCH molecules. We demonstrated that in toluene, the 4 ML CdSe NPLs form long stacks that tend to collapse into smaller fragments upon fast evaporation of the solvent, while in MCH, they remain well-dispersed. This behavior can substantially influence the solution processability of the individual components and affect the properties of the functional structures and devices. It can affect the structure and its homogeneity of the deposited NPLs' assemblies and roughness that significantly impacts, for example, the polarization of the ASE.[96] It can also impact the efficiency of the of the post-preparative chemical processes involved in chemical manipulations, for example, surface modification or synthesis via cation exchange reactions.[55]

While oleic acid stabilized quasi-spherical NPs form stable colloidal solutions in toluene,[5] that is one of the most common solvent for a broad range of colloidal NPs synthetized in nonpolar solvents, CdSe NPLs are found to form micron long ribbons in toluene. Through MD simulations,

View Article Online
DOI: 10.1039/D6NR00826G

we identified that toluene results in more extended and more solvated ligand shells and a bimodal distribution of spans of surface oleate in MCH. The drastic difference in the stacking behavior of CdSe NPLs in toluene and MCH opens the possibility to control the stacking by adjusting the composition and the solvents' ratio in solvent mixtures. We also demonstrate that solvation of the ligand shell can influence the deformation of CdSe NPLs, which, in turn, can induce strain. In the case of NPLs, this strain can contribute to the formation of a dipole moment, ultimately affecting interparticle interactions. The strains can also affect the chemical activity of the NPLs.[97, 98] Furthermore, we speculate that self-assembled configurations may enhance the material's optical performance, particularly in ASE. Notably, CdSe NPLs assembled from toluene exhibit a low ASE threshold of 14 μJ/cm² that is comparable with value obtained on assemblies obtained from more sophisticated CdSe/CdS core/shell NPLs. The samples in which the NPL arrangement was altered during storage do not exhibit ASE, thereby directly highlighting the importance of structural order for ASE values. This study further emphasizes the need to view the ligand shell as a composite ligand-solvent corona, not a dry monolayer of ligands and offers valuable insights into the solvent-dependent behavior of CdSe NPLs, which can inform the design of functional optical structures for applications such as lasing and optoelectronic devices as well as guide the solvent choice for cation exchange reaction in NPLs.

METHODS

Chemical reagents. Sodium myristate (≥99%), cadmium(II) acetate ($Cd(OAc)_2$; 99.995%), cadmium acetate dihydrate ($Cd(OAc)_2.2H_2O$), selenium powder (Se, ≥99.5%), octadecene (ODE; 90%), oleic acid (90%), toluene (98%), anhydrous isopropanol (99.8%), and anhydrous methanol were purchased from Sigma Aldrich. All chemicals were used without further purification.

Preparation of cadmium myristate. Cadmium nitrate tetrahydrate (1.23 g) was dissolved in 40 mL of methanol and 3.13 g of sodium myristate was dissolved in 250 mL of methanol under strong stirring; these solutions were then combined and stirred for approximately one hour. The whitish product was centrifuged at 6000 rpm for 10 minutes, the supernatant was discarded, and the white precipitate part was dissolved in 20 mL of methanol. The resulting precipitate of cadmium myristate was filtered and washed several times with methanol for the removal of excess precursors and the finally obtained precipitate was dried for 24 h under vacuum.

View Article Online
DOI: 10.1039/D6NR00826G

Synthesis of 4 ML CdSe NPLs. The synthesis was performed according to literature[5]. Cadmium myristate (340 mg), 24 mg Se, and ODE (30 mL) were added in a three-neck 100mL flask. The solution was degassed under vacuum at 95 °C for1.5 h. Then, the temperature of the solution was set to 240 °C under argon flow with 30 °C/min heating ramp rate. When the temperature reached 190 °C, 120 mg of cadmium acetate dihydrate powder was swiftly added. After 10 min growth at 240 °C, the solution was cooled to room temperature by removing the heating mantle and using a heat gun in ambient/cold mode to quickly bring down the temperature. When the temperature drops down to 100 °C, 2 mL of oleic acid was added to the flask.

Purification of post-synthesis byproducts and size selection of NPLs. After the synthesis, the reaction solution contains small fractions of 3 ML and 5 ML CdSe NPLs and therefore, we applied additional purification steps to remove by-products of 4 ML CdSe NPLs. For that when the solution reached room temperature, 15 mL of hexane was added. The mixture was then centrifuged at 5000 rpm for 10 min. The precipitate containing the NPLs was resuspended in 40 mL of toluene and hexane in 1:1 ratio and let sit for 2h. Most of the quantum dots (red, emitting at 550 nm) were removed through another centrifugation procedure at 5000 rpm at 10 minutes, as a reddish supernatant while the 3 ML and 4 ML NPLs are collected as precipitate. The resultant dispersion was subjected to centrifugation at 5000 rpm for 10 minutes twice, to remove reaction byproducts.

For size selection between the 4 ML and 3 ML CdSe NPLs, the precipitate from the earlier steps was redispersed in 15 mL n-hexane with 2 mL ethanol and centrifuged again at 3000 rpm for 20 minutes. The yellow supernatant, containing 4 ML CdSe NPLs, was collected and stored at room temperature until remaining 3 ML NPLs precipitated from the n-hexane dispersion, approximately within 1-2 weeks. Then, agglomerated 3 ML CdSe NPLs were removed by centrifugation at 5000 rpm for 5 minutes. 4 ML CdSe NPLs in the supernatant were precipitated to remove remaining 1-octadecene by adding 5 mL of methyl acetate and storing the dispersion in a fridge at 5 °C for 4 hours. After another centrifugation step at 5000 rpm for 5 minutes with 10% volume fraction of ethanol added to hexane, the precipitate of 4 ML CdSe NPLs was collected, redispersed in 20 mL toluene, and then stored at room temperature.

Synthesis of 3 ML CdSe NPLs. The synthesis was performed according to literature.[99] In a 100 mL three-neck flask, 14 mL of 1-octadecene (ODE), 185 mg of cadmium acetate dihydrate, and 190 µL of oleic acid were mixed and degassed for 30 min. The solution was heated to 220 °C

View Article Online
DOI: 10.1039/D6NR00826G

under argon. At temperature, 300 μL of 1 M TOP–Se was injected. The reaction mixture was kept at 220 °C for 10 min, resulting in formation of 3 ML CdSe NPLs. At the end of the growth, 2 mL oleic acid was added, and then the mixture was cooled to room temperature. The NPLs were purified by centrifugation, redispersed in hexane, precipitated with ethanol, and finally dispersed in toluene or MCH.

Synthesis of 5 ML CdSe NPLs. The synthesis was performed according to literature.[99] 340 mg of cadmium myristate and 28 mL of ODE are loaded into a 50 mL three-neck flask. The solution is stirred and degassed at room temperature for 30 min and at 95 °C for an hour under vacuum, respectively. After heater is set to 250 °C, the vacuum is broken at 100 °C and the flask is filled with argon gas. When the temperature of the solution reaches 250 °C, a pre-prepared solution of 24 mg Se dispersed in 2 mL of ODE is swiftly injected into the hot solution. When the color of solution becomes orange, 240 mg of cadmium acetate dehydrate is rapidly introduced. Then, the solution is kept at 250 °C for 10 minutes and 1 mL of OA is injected before cooling down to room temperature using water bath. After size-selective precipitation, the 5 ML NPLs are dissolved and stored in toluene or MCH.

Optical absorption and photoluminescence spectroscopy. Absorption spectra were recorded using an Agilent Technologies Cary 60 UV-Vis spectrophotometer. Photoluminescence spectra were recorded using a Fluorolog iHR 320 Horiba Jobin Yvon spectrofluorometer equipped with a PMT detector. Excitation wavelength was set at 420 nm.

Self-assembly experiments. 2 mL of CdSe NPLs toluene solution was added to the crystallization tube. After that 2 mL of methanol was carefully added on the top of the toluene solution avoiding the mixing of their interface. In ~2 weeks the CdSe NPLs were completely precipitated in a form of continuous film on the glass surface of the crystallization tube and inserted glass strip.

Small-angle x-ray scattering. SAXS data were measured for solution samples in a capillary of 1.5 mm diameter or for self-assembled structures adhered to glass cover slip at 12-ID-B beamline at the Advanced Photon Source in the Argonne National Laboratory. For solution measurements, an X-ray beam with energy of 14 keV, or wavelength $\lambda = 0.8856$ Å, and size of 300×100 μm^2 was used, with each sample typically exposed to the beam for a few seconds. The scattering data were

View Article Online
DOI: 10.1039/D6NR00826G

collected with a Pilatus2M detector located about 2 m away from the samples. Absolute intensity was calculated using water as a standard.

Transmission electron microscopy imaging. TEM images of CdSe NPLs were recorded on a Talos microscope at 200 kV acceleration voltage. Samples for the ex-situ studies were prepared by drop-casting NPLs from solution onto ultrathin carbon 300-mesh Au/400-mesh Ni grids from Ted Pella followed by drying under vacuum overnight. For liquid cell experiments, a drop of the solvent (toluene, methylcyclohexane or 1-butanol) containing the 4 ML NPLs were loaded into two graphene TEM grids and directly mounted onto the Talos double-tilt TEM holder. TEM imaging was carried out in the STEM mode and videos were captured using the Velos software.

Molecular Dynamics (MD) Simulations: Molecular dynamics (MD) simulations of CdSe nanoplatelets (NPLs) coated with oleate ligands were performed using the LAMMPS software package. All ligand and solvent atoms were explicitly included in the molecular model.[100] The OPLS-AA force field,[101] with parameters obtained from the LigParGen web server,[102-104] was used to model the interactions for both ligand and solvent atoms. For CdSe, the interaction potential consisted of a shortrange 12-6 Lennard-Jones term combined with a long-range Coulombic contribution, with parameters taken from Rabani's work.[105] Lennard-Jones parameters between the CdSe atoms and the atoms from the ligands and the solvent were obtained using the geometric mixing rule. CdSe NPLs with Cd-terminated [001] polar surfaces were constructed by first placing the Cd and Se atoms on a zinc blende lattice and then cutting the structures with a set of parallel planes to obtain the desired number of monolayers (MLs) and lateral dimensions. In this work, we have considered 4 ML NPLs with lateral extents of 24x8 nm (rectangular), such that the (110) direction made an angle of 45^{o} with the NPL edge. Sufficient number of oleate ligands were placed randomly within a thin shell surrounding the NPL to ensure charge-neutrality (~3.27 ligands/nm^2) and the resulting structure was placed at the center of a simulation box filled with solvent molecules. The arrangement the ligand as well as the solvent molecules was carried out using the PACKMOL software package.[106] The simulation box size was chosen to be big enough such that all NPL edges were at least 7 nm away from the boundary. For example, for a 4 ML 24x8 nm NPL, the box size was 38x11x11nm; with methyl cyclohexane as the solvent, that would bring the system size to ~1.9 million atoms. Periodic boundary conditions were applied along all three dimensions. The initial configuration was relaxed via a series of steps. Holding the positions of the crystal atoms fixed, we performed: (i) a step-limited constant energy run for 40 ps followed by

View Article Online
DOI: 10.1039/D6NR00826G

energy minimization to remove any significant overlap of the atoms; (ii) a temperature ramp-up to 298 K over 30 ps; (iii) further relaxation at 298 K for 30 ps; and (iv) relaxation at 298 K and 1 atm pressure for 30 ps. During these steps, the temperature was controlled by a Langevin thermostat and the pressure by a Berendsen barostat. Next, the entire system (including the crystal) was relaxed at 298K and 1 atm using a Nosé-Hoover thermostat and barostat for 200 ps, and finally followed by a production run of at least 5ns, depending on the NPL size and whether significant fluctuations persisted in the resulting configurations. The configurations were sampled every 10 ps. All results presented here have been averaged over all the sampled configurations. The equations of motion[107] were integrated by a Verlet-like scheme[108] with a time step of 1 fs during steps (i)–(iv) and 0.25 fs for the rest. Simulations performed to determine the ligand and solvent density profiles hold the crystal atom positions fixed throughout. Some runs were also performed in the absence of any solvent for comparison purposes. For simulation runs where the crystal atom position were allowed to evolve in time, the NPLs exhibit a helicoidal configuration after relaxation. The pitch corresponding to the helicoid twist was calculated based on the linear relation between the angular displacement of the midplane surface normal with the distance along the centerline. The method for reconstructing the midplane from the atom positions is discussed in Ref.[54]

ASSOCIATED CONTENT

Supporting Information. Size-selection protocol for 4 ML CdSe NPLs; The SAXS spectra measured for 5 ML and 3 ML CdSe NPLs dispersed in MCH and in toluene; dark-field STEM images of a different 4 ML CdSe NPLs sample in toluene loaded in liquid cell; high resolution images of the MD snapshots for 4 ML CdSe NPLs with oleic acid ligands and with ligand stripped; HRTEM images of 4 ML CdSe NPLs deposited from toluene solutions; summary of the SAXS data on destabilization of 4 ML CdSe NPLs in MCH by isopropanol and methanol; two-dimensional SAXS pattern measured on self-assembled 4 ML CdSe NPLs after 6 months of storage in glovebox; two-dimensional SAXS pattern measured on the film prepared by the evaporation of the toluene solution of 4 ML CdSe NPLs.

AUTHOR INFORMATION

*** Correspondence to: Elena V. Shevchenko**

View Article Online
DOI: 10.1039/D6NR00826G

Author Contributions

P.B., B.T.D., P.C.d.S.C., B.W. and R.V. performed synthesis. P. B. provided the UV-Vis, PL, and dry state TEM characterization of samples. P.B and E.V.S performed data analyses and wrote the manuscript. S.D. performed MD simulations and data analysis and B.A supervised the computational part of the study and the 3 and 5 ML work. Y.L., J.G.W and P.B. conducted the liquid cell and aberration corrected microscopy studies. C.E.R. and R.S. conducted lasing experiments and analyzed data. P.B., E.V.S, X. Z., R.V., B.A. and B.L. conducted SAXS experiments. B.L and B.A. provided analysis of SAXS data. X.M.L, E.V.S. provided project guidance. P.B. and E.V.S prepared the manuscript with the input of all co-authors. All authors have given approval to the final version of the manuscript.

Funding Sources

Work performed at the Center for Nanoscale Materials, a U.S. Department of Energy Office of Science User Facility, was supported by the U.S. DOE, Office of Basic Energy Sciences, under Contract No. DE-AC02-06CH11357. This article is part of a project that has received funding from the European Research Council under the European Union's Horizon 2020 research and innovation program (Grant agreement No. 865995). This work was granted access to the HPC resources of Institut du Développement et des Ressources en Informatique Scientifique (IDRIS) under the allocation 2024-AD010913529R2 made by Grand Équipment National de Calcul Intensif (GENCI) and was supported by the LABEX iMUST of the University of Lyon (ANR-10-LABX-0064), created within the program « Investissements d'Avenir » set up by the French government and managed by the French National Research Agency (ANR). We also gratefully acknowledge support from the PSMN (Pôle Scientifique de Modélisation Numérique) computing centre of the École Normale Supériure de Lyon.

REFERENCES

(1) Watkins, N. E.; Guan, J.; Diroll, B. T.; Williams, K. R.; Schaller, R. D.; Odom, T. W. Surface Normal Lasing from CdSe Nanoplatelets Coupled to Aluminum Plasmonic Nanoparticle Lattices. *The Journal of Physical Chemistry C* **2021**, *125* (36), 19874–19879. DOI: 10.1021/acs.jpcc.1c05662.

View Article Online
DOI: 10.1039/D6NR00826G

(2) Zhang, L.; Yang, H.; Yu, B.; Tang, Y.; Zhang, C.; Wang, X.; Xiao, M.; Cui, Y.; Zhang, J. Low-Threshold Amplified Spontaneous Emission and Lasing from Thick-Shell CdSe/CdS Core/Shell Nanoplatelets Enabled by High-Temperature Growth. *Advanced Optical Materials* **2020**, *8* (4), 1901615. DOI: https://doi.org/10.1002/adom.201901615.
(3) Guzelturk, B.; Kelestemur, Y.; Olutas, M.; Delikanli, S.; Demir, H. V. Amplified Spontaneous Emission and Lasing in Colloidal Nanoplatelets. *ACS Nano* **2014**, *8* (7), 6599–6605. DOI: 10.1021/nn5022296.
(4) She, C.; Fedin, I.; Dolzhnikov, D. S.; Dahlberg, P. D.; Engel, G. S.; Schaller, R. D.; Talapin, D. V. Red, Yellow, Green, and Blue Amplified Spontaneous Emission and Lasing Using Colloidal CdSe Nanoplatelets. *ACS Nano* **2015**, *9* (10), 9475–9485. DOI: 10.1021/acsnano.5b02509.
(5) Lee, B.; Littrell, K.; Sha, Y.; Shevchenko, E. V. Revealing the Effects of the Non-solvent on the Ligand Shell of Nanoparticles and Their Crystallization. *Journal of the American Chemical Society* **2019**, *141* (42), 16651–16662. DOI: 10.1021/jacs.9b06010.
(6) Gao, Y.; Weidman, M. C.; Tisdale, W. A. CdSe Nanoplatelet Films with Controlled Orientation of their Transition Dipole Moment. *Nano Lett.* **2017**, *17* (6), 3837–3843. DOI: 10.1021/acs.nanolett.7b01237.
(7) Momper, R.; Zhang, H.; Chen, S.; Halim, H.; Johannes, E.; Yordanov, S.; Braga, D.; Blülle, B.; Doblas, D.; Kraus, T.; et al. Kinetic Control over Self-Assembly of Semiconductor Nanoplatelets. *Nano Lett.* **2020**, *20* (6), 4102–4110. DOI: 10.1021/acs.nanolett.9b05270.
(8) Vasilopoulou, M.; Fakharuddin, A.; García de Arquer, F. P.; Georgiadou, D. G.; Kim, H.; Mohd Yusoff, A. R. b.; Gao, F.; Nazeeruddin, M. K.; Bolink, H. J.; Sargent, E. H. Advances in solution-processed near-infrared light-emitting diodes. *Nature Photonics* **2021**, *15* (9), 656–669. DOI: 10.1038/s41566-021-00855-2.
(9) Liu, J.; Guillemeney, L.; Abécassis, B.; Coolen, L. Long Range Energy Transfer in Self-Assembled Stacks of Semiconducting Nanoplatelets. *Nano Lett.* **2020**, *20* (5), 3465–3470. DOI: 10.1021/acs.nanolett.0c00376.
(10) Erdem, O.; Olutas, M.; Guzelturk, B.; Kelestemur, Y.; Demir, H. V. Temperature-Dependent Emission Kinetics of Colloidal Semiconductor Nanoplatelets Strongly Modified by Stacking. *The Journal of Physical Chemistry Letters* **2016**, *7* (3), 548–554. DOI: 10.1021/acs.jpclett.5b02763.
(11) Guzelturk, B.; Olutas, M.; Delikanli, S.; Kelestemur, Y.; Erdem, O.; Demir, H. V. Nonradiative energy transfer in colloidal CdSe nanoplatelet films. *Nanoscale* **2015**, *7* (6), 2545–2551, 10.1039/C4NR06003B. DOI: 10.1039/C4NR06003B.
(12) Abécassis, B.; Tessier, M. D.; Davidson, P.; Dubertret, B. Self-Assembly of CdSe Nanoplatelets into Giant Micrometer-Scale Needles Emitting Polarized Light. *Nano Lett.* **2014**, *14* (2), 710–715. DOI: 10.1021/nl4039746.
(13) Graf, R. T.; Schlosser, A.; Zámbó, D.; Schlenkrich, J.; Rusch, P.; Chatterjee, A.; Pfnür, H.; Bigall, N. C. Interparticle Distance Variation in Semiconductor Nanoplatelet Stacks. *Adv. Funct. Mater.* **2022**, *32* (24), 2112621. DOI: https://doi.org/10.1002/adfm.202112621.
(14) Graf, R. T.; Tran, K.; Rosebrock, M.; Borg, H.; Schlenkrich, J.; Lübkemann-Warwas, F.; Renz, F.; Dorfs, D.; Bigall, N. C. Self-Assembly of Semiconductor Nanoplatelets into Stacks

View Article Online
DOI: 10.1039/D6NR00826G

Directly in Aqueous Solution. *Advanced Materials Interfaces* **2023**, *10* (35), 2300408. DOI: https://doi.org/10.1002/admi.202300408.

(15) Antanovich, A.; Prudnikau, A.; Matsukovich, A.; Achtstein, A.; Artemyev, M. Self-Assembly of CdSe Nanoplatelets into Stacks of Controlled Size Induced by Ligand Exchange. *The Journal of Physical Chemistry C* **2016**, *120* (10), 5764–5775. DOI: 10.1021/acs.jpcc.5b12139.

(16) Schulz, F.; Lokteva, I.; Parak, W. J.; Lehmkühler, F. Recent Notable Approaches to Study Self-Assembly of Nanoparticles with X-Ray Scattering and Electron Microscopy. *Particle & Particle Systems Characterization* **2021**, *38* (9), 2100087. DOI: https://doi.org/10.1002/ppsc.202100087.

(17) Marino, E.; LaCour, R. A.; Moore, T. C.; van Dongen, S. W.; Keller, A. W.; An, D.; Yang, S.; Rosen, D. J.; Gouget, G.; Tsai, E. H. R.; et al. Crystallization of binary nanocrystal superlattices and the relevance of short-range attraction. *Nature Synthesis* **2024**, *3* (1), 111–122. DOI: 10.1038/s44160-023-00407-2.

(18) Hartley, C. L.; Kessler, M. L.; Dempsey, J. L. Molecular-Level Insight into Semiconductor Nanocrystal Surfaces. *Journal of the American Chemical Society* **2021**, *143* (3), 1251–1266. DOI: 10.1021/jacs.0c10658.

(19) Jiang, Z.; He, J.; Deshmukh, S. A.; Kanjanaboos, P.; Kamath, G.; Wang, Y.; Sankaranarayanan, S. K. R. S.; Wang, J.; Jaeger, H. M.; Lin, X.-M. Subnanometre ligand-shell asymmetry leads to Janus-like nanoparticle membranes. *Nature Materials* **2015**, *14* (9), 912–917. DOI: 10.1038/nmat4321.

(20) Shevchenko, E. V.; Talapin, D. V.; Murray, C. B.; O'Brien, S. Structural characterization of self-assembled multifunctional binary nanoparticle superlattices. . *Journal of the American Chemical Society* **2006**, *128*, 3620–3637.

(21) Shevchenko, E. V.; Talapin, D. V.; Kotov, N. A.; O'Brien, S.; Murray, C. B. Structural diversity in binary nanoparticle superlattices. *Nature* **2006**, *439*, 55. DOI: 10.1038/nature04414

https://www.nature.com/articles/nature04414#supplementary-information.

(22) Shevchenko, E. V.; Podsiadlo, P.; Wu, X.; Lee, B.; Rajh, T.; Morin, R.; Pelton, M. Visualizing Heterogeneity of Monodisperse CdSe Nanocrystals by Their Assembly into Three-Dimensional Supercrystals. *ACS Nano* **2020**, *14* (11), 14989–14998. DOI: 10.1021/acsnano.0c04864.

(23) Monego, D.; Kister, T.; Kirkwood, N.; Doblas, D.; Mulvaney, P.; Kraus, T.; Widmer-Cooper, A. When Like Destabilizes Like: Inverted Solvent Effects in Apolar Nanoparticle Dispersions. *ACS Nano* **2020**, *14* (5), 5278–5287. DOI: 10.1021/acsnano.9b03552.

(24) Winslow, S. W.; Shcherbakov-Wu, W.; Liu, Y.; Tisdale, W. A.; Swan, J. W. Characterization of colloidal nanocrystal surface structure using small angle neutron scattering and efficient Bayesian parameter estimation. *The Journal of Chemical Physics* **2019**, *150* (24). DOI: 10.1063/1.5108904 (accessed 4/9/2025).

(25) Kaushik, A. P.; Clancy, P. Solvent-driven symmetry of self-assembled nanocrystal superlattices—A computational study. *J. Comput. Chem.* **2013**, *34* (7), 523–532. DOI: https://doi.org/10.1002/jcc.23152.

(26) De Roo, J.; Yazdani, N.; Drijvers, E.; Lauria, A.; Maes, J.; Owen, J. S.; Van Driessche, I.; Niederberger, M.; Wood, V.; Martins, J. C.; et al. Probing Solvent–Ligand Interactions in Colloidal

View Article Online
DOI: 10.1039/D6NR00826G

Nanocrystals by the NMR Line Broadening. *Chem. Mater.* **2018**, *30* (15), 5485–5492. DOI: 10.1021/acs.chemmater.8b02523.

(27) Lee, J.; Lu, Z.; Wu, Z.; Ophus, C.; Schenter, G. K.; De Yoreo, J. J.; Chun, J.; Li, D. Defect Self-Elimination in Nanocube Superlattices Through the Interplay of Brownian, van der Waals, and Ligand-Based Forces and Torques. *ACS Nano* **2024**, *18* (47), 32386–32400. DOI: 10.1021/acsnano.3c08610.

(28) Price, E. K.; Bejar, G.; Kwag, J.; Brown, N.; He, L.; Tisdale, W. A. Ligand Shell Thickness of Colloidal Nanocrystals: A Comparison of Small-Angle Neutron and X-ray Scattering. *Journal of the American Chemical Society* **2025**, *147* (16), 13859–13870. DOI: 10.1021/jacs.5c02070.

(29) Missoni, L. L.; Upah, A.; Zaldívar, G.; Travesset, A.; Tagliazucchi, M. Solvent Isotherms and Structural Transitions in Nanoparticle Superlattice Assembly. *Nano Lett.* **2024**, *24* (17), 5270–5276. DOI: 10.1021/acs.nanolett.4c00875.

(30) Liu, L.; Li, C.; Fan, Z. Ligand Packing Dictates Interparticle "Bonding" in Nanoparticle Self-Assembled Structures. *ACS Materials Letters* **2025**, *7* (6), 2165–2171. DOI: 10.1021/acsmaterialslett.5c00190.

(31) Hasan, M. R.; Niebuur, B.-J.; Siebrecht, M.; Kuttich, B.; Schweins, R.; Widmer-Cooper, A.; Kraus, T. The Colloidal Stability of Apolar Nanoparticles in Solvent Mixtures. *ACS Nano* **2023**, *17* (10), 9302–9312. DOI: 10.1021/acsnano.3c00812.

(32) Li, C.; Liu, L.; Zhang, Z.; Zhang, D.; Yi, S.; Yang, H.; Fan, Z. Anisotropy in Near-Spherical Colloidal Nanoparticles. *ACS Nano* **2023**, *17* (18), 17873–17883. DOI: 10.1021/acsnano.3c03466.

(33) Li, C.; Lu, Y.; Liu, L.; Deng, M.; Fan, Z. A Particle-Based Implicit Solvent Model for Short-Range Oscillatory Solvation Forces. *Journal of Chemical Theory and Computation* **2025**, *21* (21), 10735–10745. DOI: 10.1021/acs.jctc.5c01267.

(34) Quan, Z.; Xu, H.; Wang, C.; Wen, X.; Wang, Y.; Zhu, J.; Li, R.; Sheehan, C. J.; Wang, Z.; Smilgies, D.-M.; et al. Solvent-Mediated Self-Assembly of Nanocube Superlattices. *Journal of the American Chemical Society* **2014**, *136* (4), 1352–1359. DOI: 10.1021/ja408250q.

(35) Kerr, R. D.; Gilbert, M. R.; Murphy, S. T. Relating the formation energies for oxygen vacancy defects to the structural properties of tungsten oxides. *Computational Materials Science* **2025**, *252*, 113781. DOI: https://doi.org/10.1016/j.commatsci.2025.113781.

(36) Weidman, M. C.; Smilgies, D.-M.; Tisdale, W. A. Kinetics of the self-assembly of nanocrystal superlattices measured by real-time in situ X-ray scattering. *Nature Materials* **2016**, *15* (7), 775–781. DOI: 10.1038/nmat4600.

(37) Wang, Z.; Bian, K.; Nagaoka, Y.; Fan, H.; Cao, Y. C. Regulating Multiple Variables To Understand the Nucleation and Growth and Transformation of PbS Nanocrystal Superlattices. *Journal of the American Chemical Society* **2017**, *139* (41), 14476–14482. DOI: 10.1021/jacs.7b06908.

(38) Weir, M. P.; Toolan, D. T. W.; Kilbride, R. C.; Penfold, N. J. W.; Washington, A. L.; King, S. M.; Xiao, J.; Zhang, Z.; Gray, V.; Dowland, S.; et al. Ligand Shell Structure in Lead Sulfide–Oleic Acid Colloidal Quantum Dots Revealed by Small-Angle Scattering. *The Journal of Physical Chemistry Letters* **2019**, *10* (16), 4713–4719. DOI: 10.1021/acs.jpclett.9b01008.

View Article Online
DOI: 10.1039/D6NR00826G

(39) Doblas, D.; Kister, T.; Cano-Bonilla, M.; González-García, L.; Kraus, T. Colloidal Solubility and Agglomeration of Apolar Nanoparticles in Different Solvents. *Nano Lett.* **2019**, *19* (8), 5246–5252. DOI: 10.1021/acs.nanolett.9b01688.
(40) Yin, J.-F.; Amidani, L.; Chen, J.; Li, M.; Xue, B.; Lai, Y.; Kvashnina, K.; Nyman, M.; Yin, P. Spatiotemporal Studies of Soluble Inorganic Nanostructures with X-rays and Neutrons. *Angew. Chem. Int. Ed.* **2024**, *63* (1), e202310953. DOI: https://doi.org/10.1002/anie.202310953.
(41) Talapin, D. V.; Shevchenko, E. V.; Murray, C. B.; Kornowski, A.; Förster, S.; Weller, H. CdSe and CdSe/CdS Nanorod Solids. *Journal of the American Chemical Society* **2004**, *126* (40), 12984–12988. DOI: 10.1021/ja046727v.
(42) Shevchenko, E.; Talapin, D.; Kornowski, A.; Wiekhorst, F.; Kötzler, J.; Haase, M.; Rogach, A.; Weller, H. Colloidal Crystals of Monodisperse FePt Nanoparticles Grown by a Three-Layer Technique of Controlled Oversaturation. *Adv. Mater.* **2002**, *14* (4), 287–290. DOI: https://doi.org/10.1002/1521-4095(20020219)14:4<287::AID-ADMA287>3.0.CO;2-6.
(43) Talapin, D. V.; Shevchenko, E. V.; Kornowski, A.; Gaponik, N.; Haase, M.; Rogach, A. L.; Weller, H. A New Approach to Crystallization of CdSe Nanoparticles into Ordered Three-Dimensional Superlattices. *Adv. Mater.* **2001**, *13* (24), 1868–1871. DOI: https://doi.org/10.1002/1521-4095(200112)13:24<1868::AID-ADMA1868>3.0.CO;2-0.
(44) Guzelturk, B.; Erdem, O.; Olutas, M.; Kelestemur, Y.; Demir, H. V. Stacking in Colloidal Nanoplatelets: Tuning Excitonic Properties. *ACS Nano* **2014**, *8* (12), 12524–12533. DOI: 10.1021/nn5053734.
(45) Jana, S.; de Frutos, M.; Davidson, P.; Abécassis, B. Ligand-induced twisting of nanoplatelets and their self-assembly into chiral ribbons. *Science Advances* **2017**, *3* (9), e1701483. DOI: 10.1126/sciadv.1701483 %J Science Advances.
(46) Kim, W. D.; Yoon, D.-E.; Kim, D.; Koh, S.; Bae, W. K.; Chae, W.-S.; Lee, D. C. Stacking of Colloidal CdSe Nanoplatelets into Twisted Ribbon Superstructures: Origin of Twisting and Its Implication in Optical Properties. *The Journal of Physical Chemistry C* **2019**, *123* (14), 9445–9453. DOI: 10.1021/acs.jpcc.8b09987.
(47) Jana, S.; Phan, T. N. T.; Bouet, C.; Tessier, M. D.; Davidson, P.; Dubertret, B.; Abécassis, B. Stacking and Colloidal Stability of CdSe Nanoplatelets. *Langmuir* **2015**, *31* (38), 10532–10539. DOI: 10.1021/acs.langmuir.5b02152.
(48) Chen, W.; Xiao, H.; Zhang, M.; Wang, C.; Chen, J.; Mao, R.; Jiang, L.; Hsu, H.-Y.; Buntine, M. A.; Shao, Z.; et al. Deciphering Surface Ligand Density of Colloidal Semiconductor Nanocrystals: Shape Matters. *Journal of the American Chemical Society* **2024**, *146* (42), 29104–29114. DOI: 10.1021/jacs.4c09592.
(49) Petersen, N.; Girard, M.; Riedinger, A.; Valsson, O. The Crucial Role of Solvation Forces in the Steric Stabilization of Nanoplatelets. *Nano Lett.* **2022**, *22* (24), 9847–9853. DOI: 10.1021/acs.nanolett.2c02848.
(50) Cho, W.; Kim, S.; Coropceanu, I.; Srivastava, V.; Diroll, B. T.; Hazarika, A.; Fedin, I.; Galli, G.; Schaller, R. D.; Talapin, D. V. Direct Synthesis of Six-Monolayer (1.9 nm) Thick Zinc-Blende CdSe Nanoplatelets Emitting at 585 nm. *Chemistry of Materials* **2018**, *30* (20), 6957–6960. DOI: 10.1021/acs.chemmater.8b02489.

View Article Online
DOI: 10.1039/D6NR00826G

(51) Dufour, M.; Izquierdo, E.; Livache, C.; Martinez, B.; Silly, M. G.; Pons, T.; Lhuillier, E.; Delerue, C.; Ithurria, S. Doping as a Strategy to Tune Color of 2D Colloidal Nanoplatelets. *ACS Applied Materials & Interfaces* **2019**, *11* (10), 10128–10134. DOI: 10.1021/acsami.8b18650.
(52) Chen, S.; Petersen, N.; Valsson, O.; Girard, M.; Wang, H. I. Understanding and Controlling the Colloidal Stability of CdSe Nanoplatelets by Solvation Force Engineering. *Journal of the American Chemical Society* **2025**, *147* (39), 35347–35354. DOI: 10.1021/jacs.5c08392.
(53) Po, H.; Dabard, C.; Roman, B.; Reyssat, E.; Bico, J.; Baptiste, B.; Lhuillier, E.; Ithurria, S. Chiral Helices Formation by Self-Assembled Molecules on Semiconductor Flexible Substrates. *ACS Nano* **2022**, *16* (2), 2901–2909. DOI: 10.1021/acsnano.1c09982.
(54) Monego, D.; Dutta, S.; Grossman, D.; Krapez, M.; Bauer, P.; Hubley, A.; Margueritat, J.; Mahler, B.; Widmer-Cooper, A.; Abécassis, B. Ligand-induced incompatible curvatures control ultrathin nanoplatelet polymorphism and chirality. *Proceedings of the National Academy of Sciences* **2024**, *121* (9), e2316299121. DOI: doi:10.1073/pnas.2316299121.
(55) Banerjee, P.; Filatov, A. S.; Zuo, X.; Diroll, B. T.; Shevchenko, E. V. Mechanistic Insights into Copper(I) and Copper(II) Cation Exchange Reactions in CdSe Nanoplatelets. *Chem. Mater.* **2023**, *35* (21), 8872–8882. DOI: 10.1021/acs.chemmater.3c01130.
(56) Lee, S.; Yoon, D.-E.; Kim, D.; Shin, D. J.; Jeong, B. G.; Lee, D.; Lim, J.; Bae, W. K.; Lim, H.-K.; Lee, D. C. Direct cation exchange of CdSe nanocrystals into ZnSe enabled by controlled binding between guest cations and organic ligands. *Nanoscale* **2019**, *11* (32), 15072–15082, 10.1039/C9NR05195C. DOI: 10.1039/C9NR05195C.
(57) Polovitsyn, A.; Dang, Z.; Movilla, J. L.; Martín-García, B.; Khan, A. H.; Bertrand, G. H. V.; Brescia, R.; Moreels, I. Synthesis of Air-Stable CdSe/ZnS Core–Shell Nanoplatelets with Tunable Emission Wavelength. *Chemistry of Materials* **2017**, *29* (13), 5671–5680. DOI: 10.1021/acs.chemmater.7b01513.
(58) Micheel, M.; Baruah, R.; Kumar, K.; Wächtler, M. Assembly, Properties, and Application of Ordered Group II–VI and IV–VI Colloidal Semiconductor Nanoparticle Films. *Advanced Materials Interfaces* **2022**, *9* (28), 2201039. DOI: https://doi.org/10.1002/admi.202201039.
(59) Ithurria, S.; Tessier, M. D.; Mahler, B.; Lobo, R. P. S. M.; Dubertret, B.; Efros, A. L. Colloidal nanoplatelets with two-dimensional electronic structure. *Nature Materials* **2011**, *10* (12), 936–941. DOI: 10.1038/nmat3145.
(60) Lokteva, I.; Dartsch, M.; Dallari, F.; Westermeier, F.; Walther, M.; Grübel, G.; Lehmkühler, F. Real-Time X-ray Scattering Discovers Rich Phase Behavior in PbS Nanocrystal Superlattices during In Situ Assembly. *Chem. Mater.* **2021**, *33* (16), 6553–6563. DOI: 10.1021/acs.chemmater.1c02159.
(61) Cherniukh, I.; Sekh, T. V.; Rainò, G.; Ashton, O. J.; Burian, M.; Travesset, A.; Athanasiou, M.; Manoli, A.; John, R. A.; Svyrydenko, M.; et al. Structural Diversity in Multicomponent Nanocrystal Superlattices Comprising Lead Halide Perovskite Nanocubes. *ACS Nano* **2022**, *16* (5), 7210–7232. DOI: 10.1021/acsnano.1c10702.
(62) Boles, M. A.; Engel, M.; Talapin, D. V. Self-Assembly of Colloidal Nanocrystals: From Intricate Structures to Functional Materials. *Chem. Rev.* **2016**, *116* (18), 11220–11289. DOI: 10.1021/acs.chemrev.6b00196.

View Article Online
DOI: 10.1039/D6NR00826G

(63) Bassani, C. L.; van Anders, G.; Banin, U.; Baranov, D.; Chen, Q.; Dijkstra, M.; Dimitriyev, M. S.; Efrati, E.; Faraudo, J.; Gang, O.; et al. Nanocrystal Assemblies: Current Advances and Open Problems. *ACS Nano* **2024**, *18* (23), 14791–14840. DOI: 10.1021/acsnano.3c10201.
(64) Jana, S.; Davidson, P.; Abécassis, B. CdSe Nanoplatelets: Living Polymers. *Angew. Chem. Int. Ed.* **2016**, *55* (32), 9371–9374. DOI: https://doi.org/10.1002/anie.201603880.
(65) Hansen, C. M.; Smith, A. L. Using Hansen solubility parameters to correlate solubility of C60 fullerene in organic solvents and in polymers. *Carbon* **2004**, *42* (8), 1591–1597. DOI: https://doi.org/10.1016/j.carbon.2004.02.011.
(66) Tirado, D. F.; Tenorio, M. J.; Cabañas, A.; Calvo, L. Prediction of the best cosolvents to solubilise fatty acids in supercritical CO2 using the Hansen solubility theory. *Chem. Eng. Sci.* **2018**, *190*, 14–20. DOI: https://doi.org/10.1016/j.ces.2018.06.017.
(67) Tirado, D.; Rousset, A.; Calvo, L. The Selective Supercritical Extraction of High-value Fatty Acids from Tetraselmis Suecica Using the Hansen Solubility Theory. *Chemical Engineering Transactions* **2019**, *75*, 133–138. DOI: 10.3303/CET1975023.
(68) Hansen, C. M. *Hansen Solubility Parameters: A User's Handbook*; CRC Press:, 2007.
(69) Soliwoda, K.; Tomaszewska, E.; Tkacz-Szczesna, B.; Mackiewicz, E.; Rosowski, M.; Bald, A.; Blanck, C.; Schmutz, M.; Novák, J.; Schreiber, F.; et al. Effect of the Alkyl Chain Length of Secondary Amines on the Phase Transfer of Gold Nanoparticles from Water to Toluene. *Langmuir* **2014**, *30* (23), 6684–6693. DOI: 10.1021/la501135q.
(70) Knauf, R. R.; Lennox, J. C.; Dempsey, J. L. Quantifying Ligand Exchange Reactions at CdSe Nanocrystal Surfaces. *Chem. Mater.* **2016**, *28* (13), 4762–4770. DOI: 10.1021/acs.chemmater.6b01827.
(71) Kister, T.; Monego, D.; Mulvaney, P.; Widmer-Cooper, A.; Kraus, T. Colloidal Stability of Apolar Nanoparticles: The Role of Particle Size and Ligand Shell Structure. *ACS Nano* **2018**, *12* (6), 5969–5977. DOI: 10.1021/acsnano.8b02202.
(72) Si, K. J.; Chen, Y.; Shi, Q.; Cheng, W. Nanoparticle Superlattices: The Roles of Soft Ligands. *Advanced Science* **2018**, *5* (1), 1700179. DOI: 10.1002/advs.201700179.
(73) Yang, Y.; Qin, H.; Jiang, M.; Lin, L.; Fu, T.; Dai, X.; Zhang, Z.; Niu, Y.; Cao, H.; Jin, Y.; et al. Entropic Ligands for Nanocrystals: From Unexpected Solution Properties to Outstanding Processability. *Nano Lett.* **2016**, *16* (4), 2133–2138. DOI: 10.1021/acs.nanolett.6b00730.
(74) Yang, Y.; Qin, H.; Peng, X. Intramolecular Entropy and Size-Dependent Solution Properties of Nanocrystal–Ligands Complexes. *Nano Letters* **2016**, *16* (4), 2127–2132. DOI: 10.1021/acs.nanolett.6b00737.
(75) Pita, I. A.; Singh, S.; Silien, C.; Ryan, K. M.; Liu, N. Heteroaggregation assisted wet synthesis of core–shell silver–silica–cadmium selenide nanowires. *Nanoscale* **2016**, *8* (2), 1200–1209, 10.1039/C5NR06615H. DOI: 10.1039/C5NR06615H.
(76) Kim, D.; Lee, D. C. Surface Ligands as Permeation Barrier in the Growth and Assembly of Anisotropic Semiconductor Nanocrystals. *The Journal of Physical Chemistry Letters* **2020**, *11* (7), 2647–2657. DOI: 10.1021/acs.jpclett.9b03052.

View Article Online
DOI: 10.1039/D6NR00826G

(77) Pang, Z.; Zhang, J.; Cao, W.; Kong, X.; Peng, X. Partitioning surface ligands on nanocrystals for maximal solubility. *Nature Communications* **2019**, *10* (1), 2454. DOI: 10.1038/s41467-019-10389-5.

(78) Freire-Fernández, F.; Sinai, N. G.; Hui Tan, M. J.; Park, S.-M.; Koessler, E. R.; Krauss, T.; Huo, P.; Odom, T. W. Room-Temperature Polariton Lasing from CdSe Core-Only Nanoplatelets. *ACS Nano* **2024**, *18* (23), 15177–15184. DOI: 10.1021/acsnano.4c03164.

(79) Yoon, D.-E.; Lee, J.; Yeo, H.; Ryou, J.; Lee, Y. K.; Kim, Y.-H.; Lee, D. C. Atomistics of Asymmetric Lateral Growth of Colloidal Zincblende CdSe Nanoplatelets. *Chem. Mater.* **2021**, *33* (12), 4813–4820. DOI: 10.1021/acs.chemmater.1c00563.

(80) Yadav, S.; Singh, A.; Thulasidharan, L.; Sapra, S. Surface Decides the Photoluminescence of Colloidal CdSe Nanoplatelets Based Core/Shell Heterostructures. *The Journal of Physical Chemistry C* **2018**, *122* (1), 820–829. DOI: 10.1021/acs.jpcc.7b09033.

(81) Guillemeney, L.; Dutta, S.; Valleix, R.; Patriarche, G.; Mahler, B.; Abécassis, B. Ligand Tail Controls the Conformation of Indium Sulfide Ultrathin Nanoribbons. *Journal of the American Chemical Society* **2024**, *146* (32), 22318–22326. DOI: 10.1021/jacs.4c04905.

(82) Castro, N.; Bouet, C.; Ithurria, S.; Lequeux, N.; Constantin, D.; Levitz, P.; Pontoni, D.; Abécassis, B. Insights into the Formation Mechanism of CdSe Nanoplatelets Using in Situ X-ray Scattering. *Nano Lett.* **2019**, *19* (9), 6466–6474. DOI: 10.1021/acs.nanolett.9b02687.

(83) Dozov, I.; Goldmann, C.; Davidson, P.; Abécassis, B. Probing permanent dipoles in CdSe nanoplatelets with transient electric birefringence. *Nanoscale* **2020**, *12* (20), 11040–11054, 10.1039/D0NR00884B. DOI: 10.1039/D0NR00884B.

(84) Talapin, D. V., Shevchenko, E. V., Murray, C. B., Titov, A. V., Kral, P. Dipole-Dipole Interactions in Nanoparticle Superlattices. *Nano Lett.* **2007**, *7*, 1213–1219

(85) Kelestemur, Y.; Shynkarenko, Y.; Anni, M.; Yakunin, S.; De Giorgi, M. L.; Kovalenko, M. V. Colloidal CdSe Quantum Wells with Graded Shell Composition for Low-Threshold Amplified Spontaneous Emission and Highly Efficient Electroluminescence. *ACS Nano* **2019**, *13* (12), 13899–13909. DOI: 10.1021/acsnano.9b05313.

(86) Foroutan-Barenji, S.; Erdem, O.; Gheshlaghi, N.; Altintas, Y.; Demir, H. V. Optical Gain in Ultrathin Self-Assembled Bi-Layers of Colloidal Quantum Wells Enabled by the Mode Confinement in their High-Index Dielectric Waveguides. *Small* **2020**, *16* (45), 2004304. DOI: https://doi.org/10.1002/smll.202004304.

(87) Zhang, Z.; Sun, H. Manipulation of the Optical Properties of Colloidal 2D CdSe Nanoplatelets. *Advanced Photonics Research* **2021**, *2* (8), 2100045. DOI: https://doi.org/10.1002/adpr.202100045.

(88) Yang, Z.; Pelton, M.; Fedin, I.; Talapin, D. V.; Waks, E. A room temperature continuous-wave nanolaser using colloidal quantum wells. *Nature Communications* **2017**, *8* (1), 143. DOI: 10.1038/s41467-017-00198-z.

(89) Belitsch, M.; Dirin, D. N.; Kovalenko, M. V.; Pichler, K.; Rotter, S.; Ghalgaoui, A.; Ditlbacher, H.; Hohenau, A.; Krenn, J. R. Gain and lasing from CdSe/CdS nanoplatelet stripe waveguides. *Micro and Nano Engineering* **2022**, *17*, 100167. DOI: https://doi.org/10.1016/j.mne.2022.100167.

View Article Online
DOI: 10.1039/D6NR00826G

(90) Ibáñez, M.; Boehme, S. C.; Buonsanti, R.; De Roo, J.; Milliron, D. J.; Ithurria, S.; Rogach, A. L.; Cabot, A.; Yarema, M.; Cossairt, B. M.; et al. Prospects of Nanoscience with Nanocrystals: 2025 Edition. *ACS Nano* **2025**, *19* (36), 31969–32051. DOI: 10.1021/acsnano.5c07838.
(91) Podsiadlo, P.; Lee, B.; Prakapenka, V. B.; Krylova, G. V.; Schaller, R. D.; Demortière, A.; Shevchenko, E. V. High-Pressure Structural Stability and Elasticity of Supercrystals Self-Assembled from Nanocrystals. *Nano Lett.* **2011**, *11* (2), 579–588. DOI: 10.1021/nl103587u.
(92) Chhantyal, P.; Naskar, S.; Birr, T.; Fischer, T.; Lübkemann, F.; Chichkov, B. N.; Dorfs, D.; Bigall, N. C.; Reinhardt, C. Low Threshold Room Temperature Amplified Spontaneous Emission in 0D, 1D and 2D Quantum Confined Systems. *Scientific Reports* **2018**, *8* (1), 3962. DOI: 10.1038/s41598-018-22287-9.
(93) She, C.; Fedin, I.; Dolzhnikov, D. S.; Demortière, A.; Schaller, R. D.; Pelton, M.; Talapin, D. V. Low-Threshold Stimulated Emission Using Colloidal Quantum Wells. *Nano Lett.* **2014**, *14* (5), 2772–2777. DOI: 10.1021/nl500775p.
(94) Diroll, B. T.; Chen, M.; Coropceanu, I.; Williams, K. R.; Talapin, D. V.; Guyot-Sionnest, P.; Schaller, R. D. Polarized near-infrared intersubband absorptions in CdSe colloidal quantum wells. *Nature Communications* **2019**, *10* (1), 4511. DOI: 10.1038/s41467-019-12503-z.
(95) Zhang, M.; Hu, J.; Xi, G.; Tu, J.; Yang, Q.; Fan, L.; Lu, Y.; Sui, M.; Sun, X.; Zhang, L.; et al. Colloidal Perovskite Nanocrystal Superlattice Films with Simultaneous Polarized Emission and Orderly Electric Polarity via an In Situ Surface Cross-Linking Reaction. *ACS Nano* **2025**, *19* (7), 7283–7293. DOI: 10.1021/acsnano.4c17654.
(96) Duan, R.; Zhang, Q.; Thung, Y. T.; Zhou, X.; Yin, T.; Ao, Y.; Xiao, L.; Zhang, Z.; Lee, C. X. X.; Ren, T.; et al. Continuous-Wave Pumped Self-Assembled Colloidal Topological Lasers. *Adv. Mater.* **2025**, *37* (11), 2416635. DOI: https://doi.org/10.1002/adma.202416635.
(97) Blomberg, S.; Zetterberg, J.; Zhou, J.; Merte, L. R.; Gustafson, J.; Shipilin, M.; Trinchero, A.; Miccio, L. A.; Magaña, A.; Ilyn, M.; et al. Strain Dependent Light-off Temperature in Catalysis Revealed by Planar Laser-Induced Fluorescence. *ACS Catalysis* **2017**, *7* (1), 110–114. DOI: 10.1021/acscatal.6b02440.
(98) Temmel, S. E.; Fabbri, E.; Pergolesi, D.; Lippert, T.; Schmidt, T. J. Investigating the Role of Strain toward the Oxygen Reduction Activity on Model Thin Film Pt Catalysts. *ACS Catalysis* **2016**, *6* (11), 7566–7576. DOI: 10.1021/acscatal.6b01836.
(99) Martinet, Q.; Baronnier, J.; Girard, A.; Albaret, T.; Saviot, L.; Mermet, A.; Abecassis, B.; Margueritat, J.; Mahler, B. Ligand-dependent nano-mechanical properties of CdSe nanoplatelets: calibrating nanobalances for ligand affinity monitoring. *Nanoscale* **2021**, *13* (18), 8639–8647, 10.1039/D1NR00270H. DOI: 10.1039/D1NR00270H.
(100) Thompson, A. P.; Aktulga, H. M.; Berger, R.; Bolintineanu, D. S.; Brown, W. M.; Crozier, P. S.; in 't Veld, P. J.; Kohlmeyer, A.; Moore, S. G.; Nguyen, T. D.; et al. LAMMPS - a flexible simulation tool for particle-based materials modeling at the atomic, meso, and continuum scales. *Comput. Phys. Commun.* **2022**, *271*, 108171. DOI: https://doi.org/10.1016/j.cpc.2021.108171.
(101) Jorgensen, W. L.; Maxwell, D. S.; Tirado-Rives, J. Development and Testing of the OPLS All-Atom Force Field on Conformational Energetics and Properties of Organic Liquids. *Journal of the American Chemical Society* **1996**, *118* (45), 11225–11236. DOI: 10.1021/ja9621760.

View Article Online
DOI: 10.1039/D6NR00826G

(102) Jorgensen, W. L.; Tirado-Rives, J. Potential energy functions for atomic-level simulations of water and organic and biomolecular systems. *Proceedings of the National Academy of Sciences* **2005**, *102* (19), 6665–6670. DOI: doi:10.1073/pnas.0408037102.
(103) Dodda, L. S.; Vilseck, J. Z.; Tirado-Rives, J.; Jorgensen, W. L. 1.14*CM1A-LBCC: Localized Bond-Charge Corrected CM1A Charges for Condensed-Phase Simulations. *The Journal of Physical Chemistry B* **2017**, *121* (15), 3864–3870. DOI: 10.1021/acs.jpcb.7b00272.
(104) Dodda, L. S.; Cabeza de Vaca, I.; Tirado-Rives, J.; Jorgensen, W. L. LigParGen web server: an automatic OPLS-AA parameter generator for organic ligands. *Nucleic Acids Res.* **2017**, *45* (W1), W331–W336. DOI: 10.1093/nar/gkx312 (accessed 2/25/2026).
(105) Rabani, E. An interatomic pair potential for cadmium selenide. *The Journal of Chemical Physics* **2002**, *116* (1), 258–262. DOI: 10.1063/1.1424321.
(106) Martínez, L.; Andrade, R.; Birgin, E. G.; Martínez, J. M. PACKMOL: A package for building initial configurations for molecular dynamics simulations. *J. Comput. Chem.* **2009**, *30* (13), 2157–2164. DOI: https://doi.org/10.1002/jcc.21224.
(107) Shinoda, W.; Shiga, M.; Mikami, M. Rapid estimation of elastic constants by molecular dynamics simulation under constant stress. *Physical Review B* **2004**, *69* (13), 134103. DOI: 10.1103/PhysRevB.69.134103.
(108) Tuckerman, M. E.; Alejandre, J.; López-Rendón, R.; Jochim, A. L.; Martyna, G. J. A Liouville-operator derived measure-preserving integrator for molecular dynamics simulations in the isothermal–isobaric ensemble. *J. Phys. A: Math. Gen.* **2006**, *39* (19), 5629. DOI: 10.1088/0305-4470/39/19/S18.

View Article Online
DOI: 10.1039/D6NR00826G

Data availability

The data supporting this article have been included as part of the ESI.